AWARD NUMBER: W81XWH-13-1-0227

TITLE: Deficient BIM Expression as a Mechanism of Intrinsic and Acquired Resistance to Targeted Therapies in EGFR-Mutant and ALK-Positive Lung Cancers

PRINCIPAL INVESTIGATOR: Lecia Sequist MD.

CONTRACTING ORGANIZATION: Massachusetts General Hospital
Boston, MA 02114

REPORT DATE: October 2016

TYPE OF REPORT: Final

PREPARED FOR: U.S. Army Medical Research and Materiel Command
Fort Detrick, Maryland 21702-5012

REPORT DOCUMENTATION PAGE

Form Approved
OMB No. 0704-0188

1. REPORT DATE	2. REPORT TYPE	3. DATES COVERED
October 2016	Final	1 Aug 2013 - 31 Jul 2016

4. TITLE AND SUBTITLE

Deficient BIM Expression as a Mechanism of Intrinsic and Acquired Resistance to Targeted Therapies in EGFR-Mutant and ALK-Positive Lung Cancers

5a. CONTRACT NUMBER

5b. GRANT NUMBER
W81XWH-13-1-0227

5c. PROGRAM ELEMENT NUMBER

6. AUTHOR(S)

Jeffrey Engelman MD PhD and Lecia Sequist MD

E-Mail: jengelman@partners.org; lsequist@partners.org

5d. PROJECT NUMBER

5e. TASK NUMBER

5f. WORK UNIT NUMBER

7. PERFORMING ORGANIZATION NAME(S) AND ADDRESS(ES)

Massachusetts General Hospital

55 Fruit St
Boston, MA 02114

8. PERFORMING ORGANIZATION REPORT NUMBER

9. SPONSORING / MONITORING AGENCY NAME(S) AND ADDRESS(ES)

U.S. Army Medical Research and Materiel Command
Fort Detrick, Maryland 21702-5012

10. SPONSOR/MONITOR'S ACRONYM(S)

11. SPONSOR/MONITOR'S REPORT NUMBER(S)

12. DISTRIBUTION / AVAILABILITY STATEMENT

Approved for Public Release; Distribution Unlimited

13. SUPPLEMENTARY NOTES

14. ABSTRACT

This project has made very good progress. We have now unveiled an even larger role for defective apoptosis in the emergence of resistance. We have been very successful in our ability to generate cell lines derived from patient biopsies both before treatment and at the time of resistance. We are now using these patient-derived cell lines to assess BIM levels and apoptotic response to next-generation inhibitors. The capacity to develop cell lines from patient biopsies was published in December, 2014 in *Science*. We have used these models to develop effective combinations to overcome the defect in apoptosis which has led to a CTEP-sponsored clinical trial combining AZD9291 and ABT-263. Our research has expanded beyond just assessing BIM, and is also focusing on the role of a diminished apoptotic response as clones develop resistance to targeted therapies. Although BIM is one such mechanism, it is not the only one. This research has uncovered a novel, unexpected connection between EMT, low BIM, and resistance to targeted therapies. Two manuscripts (one under review at *Nature Communications* and one to be submitted) have been written this year describing our findings.

15. SUBJECT TERMS

BIM, apoptosis, targeted therapy, BCL-XL, kinase, EGFR, ALK, lung cancer

16. SECURITY CLASSIFICATION OF:			17. LIMITATION OF ABSTRACT	18. NUMBER OF PAGES	19a. NAME OF RESPONSIBLE PERSON
a. REPORT	b. ABSTRACT	c. THIS PAGE			USAMRMC
Unclassified	Unclassified	Unclassified	Unclassified	27	19b. TELEPHONE NUMBER *(include area code)*

Table of Contents

Page

1. INTRODUCTION: Narrative that briefly (one paragraph) describes the subject, purpose and scope of the research.

In lung cancers that have oncogene-addiction to a specific kinase, inhibition of that kinase often leads to cell growth arrest and apoptosis. For example, *EGFR* mutant and *EML4-ALK* lung cancers have been proven highly sensitive to the corresponding specific tyrosine kinase inhibitors (TKIs). Although cancers with these genetic abnormalities often respond to the appropriate targeted therapy, there is marked heterogeneity in degree of clinical benefit. We hypothesized that that some oncogene-addicted cancers are poised to undergo apoptosis following treatment, whereas others are not; and expression of the critical pro-apoptotic protein BIM in pre-treatment biopsies may distinguish patients who have impressive, durable responses from those who have weak, transient responses. Our original project aimed to assess *EGFR* mutant and *EML4-ALK* lung cancer specimens to determine if low basal BIM expression predicts a poorer clinical outcome to TKIs.

2.KEYWORDS: Provide a brief list of keywords (limit to 20 words).

BIM, apoptosis, targeted therapy, BCL-XL, kinase, EGFR, ALK, lung cancer

3.OVERALL PROJECT SUMMARY: Our award period ended 7/31/2016. Of note, my co-PI Dr. Engelman left MGH to take a new role at Novartis as of 6/16/2016 so this report will serve as the final scientific report for both of the PI's on this award.

Over the 3-year period of this award, this project was very successful. Our capacity to develop cell lines from patient biopsies was published in December 2014 in *Science*. We have been able to use these models integrally in our research to assess apoptotic response to next-generation inhibitors, including the development of effective combinations to overcome defects in apoptosis. These findings have led to a CTEP-sponsored clinical trial combining AZD9291 and ABT-263 which opened for patient accrual in September 2016 and is now enrolling at 7 cancer centers across the country.

Importantly, we have now unveiled an even larger role for defective apoptosis in the emergence of resistance (ie, broader than BIM alone) and published some of these findings in *Nature Medicine* in March 2016, with a second related manuscript currently in preparation. Our research has now expanded beyond just assessing BIM and is focusing on the roles of a diminished apoptotic response and epithelial to mesenchymal transformation as clones develop resistance to targeted therapies. Although loss of BIM is one such mechanism to impaired apoptosis, it is not the only one. We are now actively trying to identify other mechanisms as well.

Since the inception of this research program, our findings have led us to appreciate the fundamental importance of diminished apoptosis in the evolution of resistance to

targeted therapies, a characteristic that is orthogonal to the more traditionally studied genetic mechanisms of drug resistance. We have gained tremendous new knowledge about this arena thanks to the funding we received from DOD. Specifically, we have studied in detail the process by which *EGFR* mutant cancers can develop the T790M resistance mutation under the selective pressure of gefitinib. We now have 2 divergent conceptual models for how cancers can develop the same T790M mutation and thus acquire resistance to EGFR-targeted therapies (Fig 1):

A. Pre-existing model: In this model, there are a subset of cells within the tumor that have a T790M mutation prior to treatment and these are simply preferentially selected by treatment with EGFR inhibitors that can't inhibit T790M (ie, 1st-line treatments).

B. Persister-evolution model: In this model, cancer cells that initially survive 1st-line therapy by virtue of entering a persister state are preferentially selected by drug treatment. **These cells do not undergo apoptosis.** During weeks and months of ongoing 1st-line therapy, these cells can develop mutations and become fully resistant. However, the tumors that evolve from these drug tolerant persister cells continue to have an apoptotic defect.

Figure 1. Two models of the development of acquired resistance to EGFR inhibitors

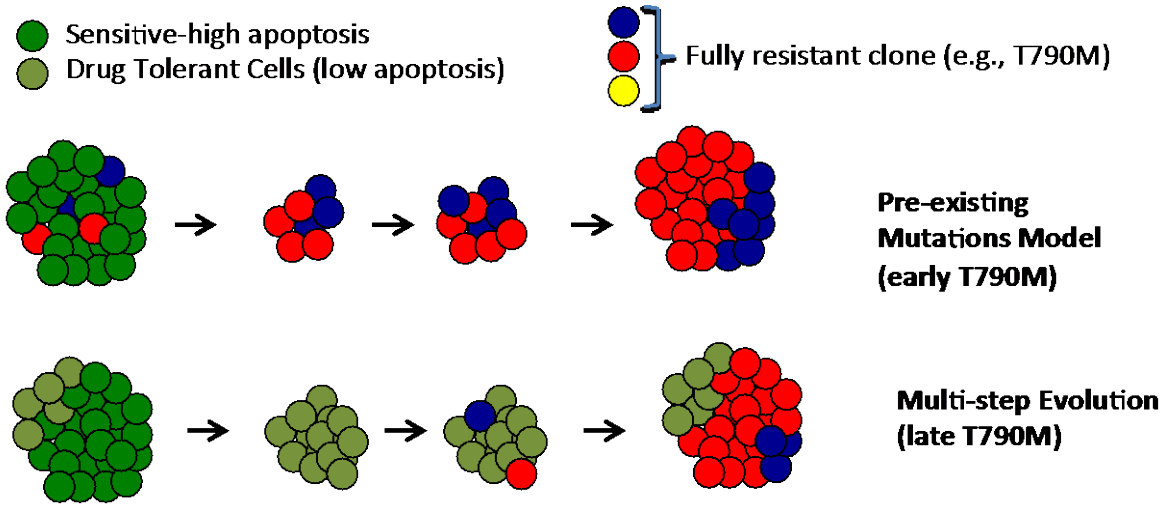

As detailed below, much of the research done through the course of this award focused on understanding if and how EGFR mutant cancers might have different apoptotic responses to 2nd and 3rd line targeted therapies depending on "how" the cancer became resistant to initial therapy, via pre-existing mutations or via multi-step evolution from persister cells. Also note that since this major breakthrough understanding about these two distinct pathways was discovered in EGFR mutant cancers, our subsequent

research focused on this disease. We hope to understand in the future if similar biology exists in ALK-translocated cancers as well.

Aim 1: Validate BIM as a biomarker that predicts outcome in patients treated with EGFR and ALK inhibitors.

Aim 1 original objectives: obtain biopsies from 100 *EGFR* mutant lung cancer patients and 60 *ALK*-translocated lung cancer specimens prior to TKI treatment on which to perform BIM IHC and RNA ISH in order to prospectively analyze the relationship between baseline BIM expression and subsequent progression-free survival (PFS).

Summary of Results, Progress and Accomplishments: Since obtaining this award we have accumulated baseline (prior to first-line treatment) material from 185 *EGFR* mutant lung cancer patients and 100 *ALK*-translocated patients, thus exceeding the number of samples planned for this grant.

We worked closely with Dr. David Rimm at Yale University to develop a robust, quantitative IHC for the detection of BIM. The assay was developed and validated using a set of 25 of paired pre/post-treatment *EGFR* mutant samples, as shown in last year's annual update.

However, while we were eagerly working to optimize and validate BIM IHC staining on *EGFR* mutant lung specimens to determine if this would lead to the use of BIM as a biomarker to predict response, the results from a post-hoc analysis of the randomized EURTAC trial were published (Costa, et al, Clinical Cancer Research, 2014). This manuscript reported the BIM mRNA expression levels in 83 pre-treatment tumor samples from *EGFR* mutant lung cancer patients receiving first-line erlotinib with the goal of assessing BIM as a predictive biomarker of progression-free survival, response rate, and overall survival. Using quantitative-PCR, BIM mRNA was analyzed in 83 specimens. BIM expression was classified as low/intermediate in 53 samples (63.96%) and high in 30 samples (36.14%). Analysis revealed that the PFS for patients with low/intermediate BIM expression treated with erlotinib was 7.2 months, while the PFS for patients with high BIM expression treated with erlotinib was 12.9 months. The response rate to erlotinib in patients with low/intermediate BIM expression was 31.58%, compared to 80% in patients with high BIM expression. The overall survival of patients following erlotinib treatment in low/intermediate BIM expressing-tumor samples was 20.8 months, with high BIM-expressing tumor samples exhibiting 24.5 months. This important paper confirmed our earlier work, and suggested baseline BIM expression levels indeed are a predictive biomarker of clinical outcome with first-line EGFR inhibitor therapy for EGFR-mutant lung cancer.

As discussed in our progress report from last year, when the Costa publication came out, we opted against continuing to attempt to duplicate efforts by assessing BIM expression in our expanded clinical panel of pre-treatment *EGFR* mutant biopsy specimens since the analysis would have been redundant. Instead we shifted our focus

toward looking at the persister drug tolerant cells we cultivated by treating with first-line inhibitors, as depicted above in Figure 1, in order to understand how BIM may be associated with apoptosis to 3rd-generation EGFR inhibitors in these models.

We found that in our two models of EGFR inhibitor acquired resistance, the cells with pre-existing T790M mutations (the early T790M model, referred to below as GR2 cells) had significant upregulation of BIM compared to the multi-step evolution persister cells (the late T790M model, referred to below as the GR3 cells), see Figure 2. The BIM-deficient GR3 cells also then had impaired BIM induction when treated with a T790M-specific 3rd-generation inhibitor, WZ4002, as shown in Figure 3.

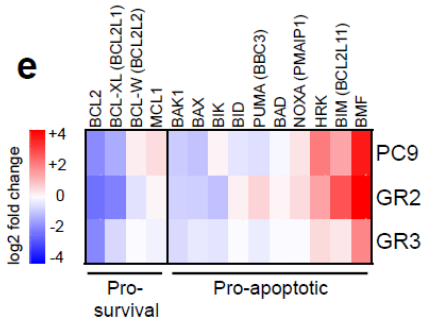

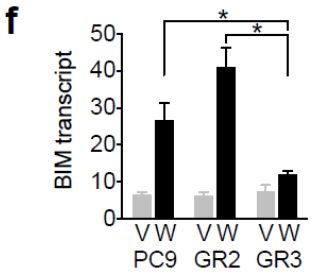

Figure 2: Compared to parental and PC9-GR2 cells, PC9-GR3 cells had diminished upregulation of BIM. Reprinted from Supplemental Figure 2 in Hata and Niederst et al. *Nature Medicine* 2016.

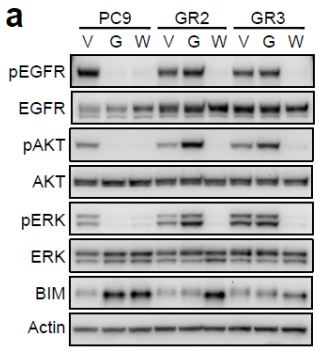

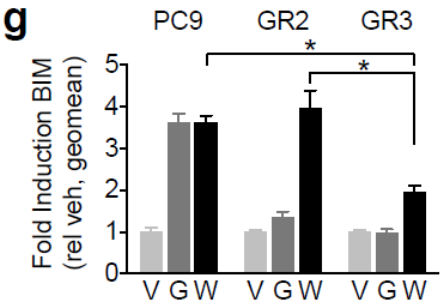

Figure 3: Induction of BIM protein levels after WZ4002 treatment was significantly lower ($P < 0.05$) in PC9-GR3 cells than in PC9-GR2 or parental cells. Reprinted from Supplemental Figure 2 in Hata and Niederst et al. *Nature Medicine* 2016.

Finally, using RNA sequencing (RNA-seq) analysis, we compared the transcriptional profiles parental PC9 cells with those of PC9-GR2 and PC9-GR3. Gene-set enrichment analysis revealed the upregulation of genes related to epithelial-to-mesenchymal transition (EMT) in drug-tolerant and PC9-GR3 cells relative to the parental and PC9-GR2 cells, Figure 4. This was a fascinating finding as we and others had previously observed that EGFR-mutant NSCLCs that have an EMT phenotype are associated with resistance to EGFR inhibtor therapy, both in the upfront setting and in the acquired resistance setting (Sequist, et al, *Science Trans Med* 2013). However, the mechanisms

underlying EMT-mediated resistance are not well-defined, limiting development of therapies to treat and/or prevent EMT.

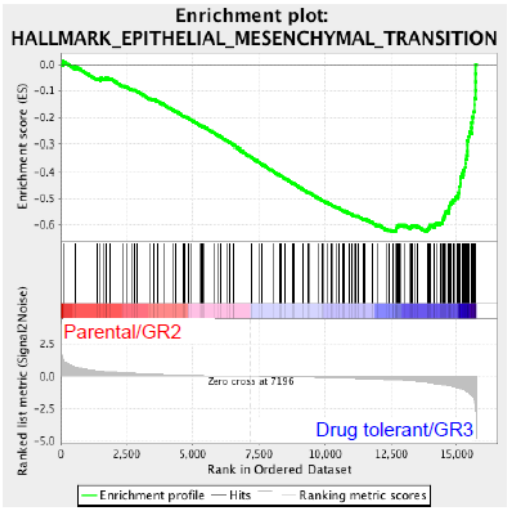

Figure 4: **Gene set enrichment analysis of global transcriptional profiles of PC9 parental, drug tolerant persister, and resistant cell lines determined by RNA-seq.** Drug tolerant persister cells and late evolving T790M resistant cells have upregulation of genes related to EMT. Reprinted from Supplemental Figure 11 in Hata and Niederst et al. *Nature Medicine* 2016

The findings above in figures 1-4 have now been published in *Nature Medicine* and taken together with the Costa paper support our original hypothesis that BIM expression is necessary for optimal apoptosis in response to targeted therapy in oncogene-addicted lung cancers. Lack of BIM and/or BIM induction with targeted therapy is associated with decreased clinical response. Furthermore, low or suppressed BIM may lie at the root of the drug-tolerant persister cell phenotype, which may be closely tied to the EMT phenotype.

Aim 2: Determine if BIM expression is lost in cancers that develop resistance to targeted therapies

Aim 2 original objectives: Interrogate cell lines made resistant to drugs *in vitro* as well as patient-derived cell lines obtained from biopsies at the time of clinically-acquired drug resistance to determine if BIM levels are reduced in resistant cell lines compared to parental cell lines, and whether resistant lines have a reduced apoptotic response to second-line targeted therapies. Our goal was to biopsy approximately 50 *EGFR* mutant lung cancer patients to get both pre- and post-treated matched specimens that have acquired resistance to TKI and approximately 30 similar *ALK* cases.

Summary of Results, Progress and Accomplishments: Since obtaining this award, we have exceeded our original goals by accumulating matched pre- and post-treatment paired tumor material from 153 *EGFR* mutant lung cancer patients and 55 *ALK*-translocated patients (see below).

Pre-EGFR TKI Specimens	Post-EGFR TKI Specimens	Paired Pre-/Post-EGFR TKI Specimens
185	262	153
Pre-ALK TKI Specimens	**Post-ALK TKI Specimens**	**Paired Pre-/Post-ALK TKI Specimens**
105	113	55

In addition, we have been very successful in our ability to generate patient-derived cell lines, as we published in Crystal, et al *Science* 2014. At the current time we have "completed", or finished/finalized over 60 cell lines from EGFR patients and over 40 from ALK patients.

Initially, for Aim 2 we looked to commercially-available cell lines and made them resistant to EGFR inhibitors *in vitro* to assess BIM and other related regulators of apoptosis. We assayed two clones from an *EGFR* mutant NSCLC cell line (H1975) that were made resistant to the EGFR T790M inhibitor PF00299804 by increasing the exposure to the clones until they grew in drug and were accordingly resistant to 3rd-generation EGFR T790M inhibitors, such as WZ4002 (Figure 5A).

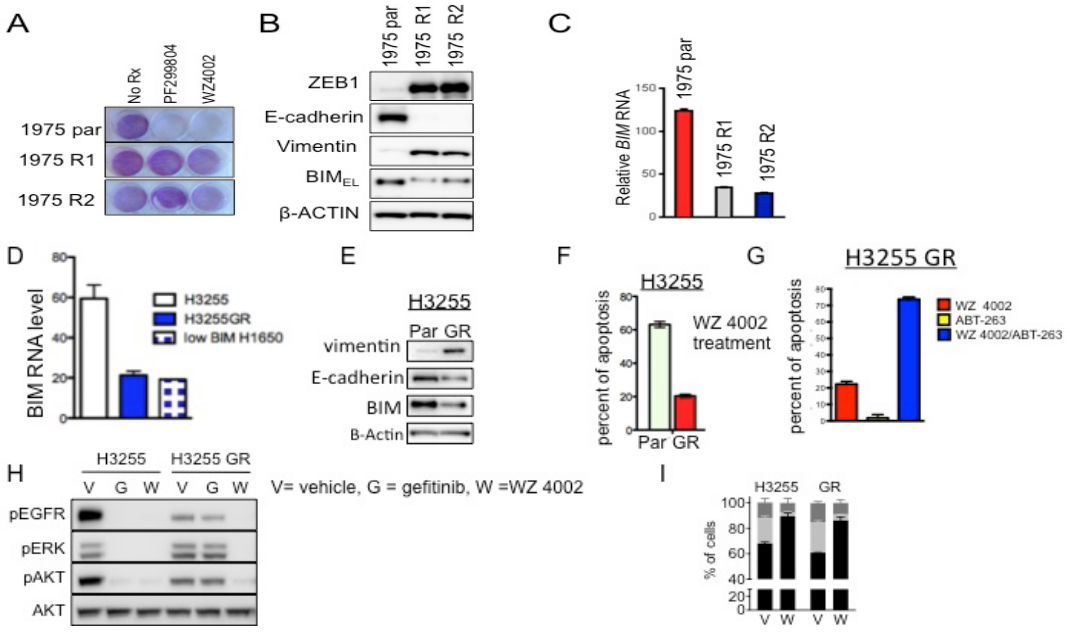

Figure 5. BIM is correlated with EMT in *EGFR* mutant lung cancer resistant models. (A) 1975R1 and R2 cells are resistant to EGFRi (B) EMT and low (B and C) BIM in R1 and R2 cells. (D-I) A second EGFRi resistant cell line, H3255 GR, has low BIM, underwent EMT, is resistant to apoptosis, sensitized to apoptosis by ABT-263, and has equivalent shutdown of intracellular signaling and growth arrest following WZ4002 treatment as the parental cells

The resistant clones R1 and R2 underwent EMT as evidenced by upregulated vimentin, ZEB1 and downregulated E-cadherin, all EMT hallmarks (Fig. 5B). We probed various BCL-2 family members and demonstrated that BIM was markedly down-regulated in the two clones that underwent EMT compared to the parental at the protein level (data not shown) and RNA level (Fig. 5C). As expected with low BIM cells, we found these cells were resistant to apoptosis following treatment with WZ4002 compared to parental cells. The expression of other BCL-2 family members we had probed besides BIM were unaltered (data not shown), further suggesting depressed BIM was playing a unique role in resistance. In a second EGFR inhibitor-resistant line, H3255GR (a model with T790M), we also observed low BIM (Fig. 5D and 5E) in parallel with EMT (Fig. 5E), and

were as a result resistant to apoptosis (Fig. 5F and 5G) despite undergoing equivalent signaling shutdown and growth arrest as the parental cells (Fig. 5H and 5I). Interestingly, the H3255GR cells were sensitized to apoptosis by the BCL-2/XL inhibitor ABT-263 (navitoclax) (Fig. 5G).

These data together suggest that the EMT phenotype correlates with a depressed apoptotic response following EGFR inhibitor treatment, and that these cells also have low BIM-mediated loss of apoptosis. These data also indicate that EGFR-mutant NSCLCs that acquire T790M may remain resistant to T790M inhibitors if they also undergo EMT, and this may be rescued by the addition of ABT-263 to the EGFR T790M inhibitor.

Interestingly, when we looked for findings similar to those observed in the H1975 cells within our patient-derived models obtained at the time of acquired drug resistance we found several of these had refractory apoptosis responses to WZ4002 (Fig. 6A). Impressively the two cancers with the lowest apoptotic responses had undergone EMT (Figs. 6A and 6B). BIM RNA levels within the mesenchymal-type cancers were significantly lower then among the more epithelial cell lines (Fig. 6C). The data generated by our work in Aims 1 and 2 both suggests that within a given molecular mechanism of acquired drug resistance like T790M, one can observe heterogeneity in biology. Specifically, the persister-phenotype cells appear to have lower BIM expression and evidence of EMT, and thus reduced apoptotic responses to both first-line and next-generation targeted therapies.

Figure 6. Mesenchymal *EGFR* mutant NSCLC patient-derived cell lines are resistant to apoptosis (A) Apoptosis of epithelial cells and mesenchymal cells (MGH125 and MGH138). All cell lines have co-T790M mutations. (B) Western blot (C) Relative Vimentin RNA in “low” BIM and med/high “BIM”. Please note: Mesenchymal cancers have low BIM.

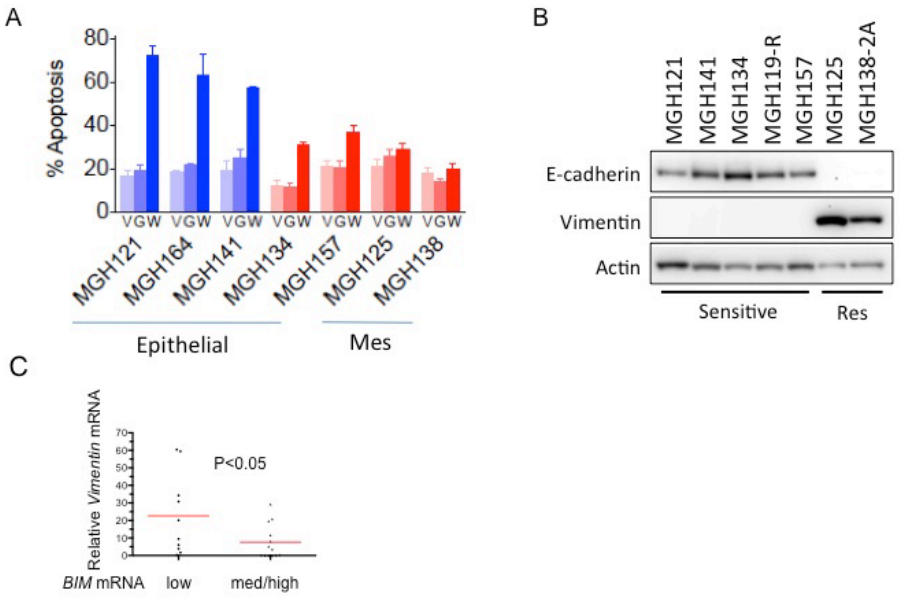

We wanted to understand the mechanistic link between BIM and EMT. The low BIM RNA levels we observed in mesenchymal cancers (Fig 5) suggested that the regulation of BIM expression may be occurring at the transcriptional level. Therefore, we hypothesized that BIM expression might be directly suppressed by transcriptional repressors that are upregulated during EMT. Using the SwissRegulon portal we searched for transcription factors associated with EMT with putative binding sites in the BIM promoter. From these analyses, we identified that the transcriptional repressor ZEB1 was a candidate to bind the BIM promoter (data not shown). To confirm a functional role for ZEB1 in suppressing BIM levels, we stably depleted ZEB1 by short hairpin (sh) RNA in the H1975 R2 model. Indeed, knockdown of ZEB1 led to an increased expression of BIM, at both the protein and RNA levels (Figure 7). Importantly, this depletion of ZEB1 also led to re-sensitization of H1975 R2 cells to EGFR inhibitors.

Figure 7: ZEB1 is an EMT marker associated with resistance to EGFRi in lung cancer and its depletion leads to BIM de-repression. qRT-PCR of BIM RNA following sh control (GFP or scrambled, (Scr), and shZEB1 introduction into 1975 R2 EMT cells (left). siScr and siZEB1 treated H1975 R2 cells were probed for ZEB1, BIM and the loading control β-Actin (midde). H1975 R2 cells transduced with two guide RNAs against ZEB1 in a lentiviral plasmid or a control lentiviral plasmid were lysed and probed with the indicated antibodies.

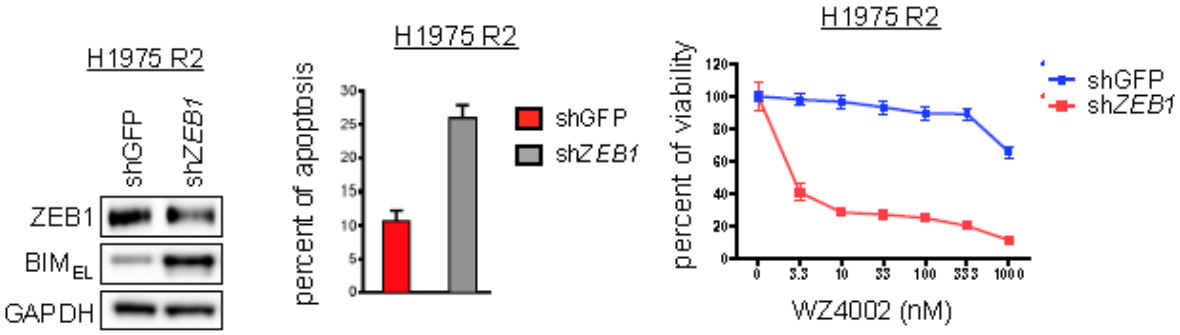

These findings represent a heretofore never described ZEB1-BIM interaction that underlies low BIM expression in NSCLCs that undergo EMT, thus revealing a commonality between the two modes of resistance. Mechanistically, depression of BIM is mediated by direct ZEB1 binding to the BIM promoter and suppressing BIM transcription. Indeed, these data may also provide critical insight into EMT-associated resistance in other settings. Our analysis of large gene expression databases has revealed that mesenchymal gene expression and BIM expression are anti-correlated across multiple solid tumor types (including *KRAS* mutant NSCLC) and ZEB1 binds to the BIM promoter in non-lung cancer cells. Furthermore,EMT is broadly associated with resistance to a number of targeted therapies, chemotherapies and radiotherapy in varied cancer types. The full extent of our findings in this realm is described in a manuscript that is currently under review.

Aim 3: Assess novel therapeutic strategies for cancers with low BIM expression that aim to increase BIM and thereby enhance response.

Aim 3 original objectives: Use cell lines to induce BIM expression using a DOX-inducible BIM expression lentivirus to confirm that this can enhance response, as well as test if epigenetic manipulation with 5'AZA and other similar compounds can induce BIM expression with similar results. Then test successful combinations *in vivo* in mice.

Summary of Results, Progress and Accomplishments: We sought to identify therapeutic strategies that could enhance the apoptotic response to third generation EGFR inhibitors. We have previously reported a drug screening strategy for identifying effective drug combinations for cancers with acquired resistance to targeted therapies. We screened four low-apoptosis T790M patient-derived cell lines (MGH134, MGH157, MGH125, and MGH138) to identify drugs that increased E_{max} when combined with WZ4002. The BCL-XL/BCL-2 inhibitor ABT263 (now called navitoclax) was shown to induce a robust apoptotic response in combination with WZ4002 in both T790M patient-derived cell lines and in *in vitro* generated T790M resistant cell lines (Figure 8). *In vivo*, WZ4002 and navitoclax in combination induced regressions in MGH134 and PC9-GR3 xenograft tumor models (Figure 9). Both figures below were reprinted from Figure 4 in Hata and Niederst et al. *Nature Medicine* 2016

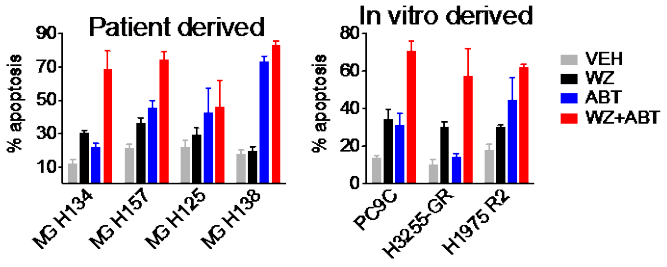

Figure 8. Combination of WZ4002 and ABT263 induces apoptosis in T790M+ cell lines with reduced apoptotic response to WZ4002 alone.

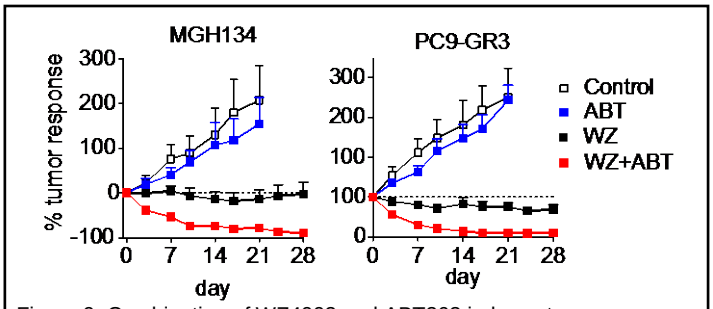

Figure 9. Combination of WZ4002 and ABT263 induces tumor regression in subcutaneous xenograft tumors established from low apoptosis T790M+ cell lines.

BH3 mimetics are effective anti-cancer drugs that work by reducing the apoptotic thresholds of cells by liberating BIM protein from complexes with the anti-apoptotic proteins BCL-2 and BCL-xL. We also treated the low BIM expressing clones H1975 R1 and H1975 R2 with ABT-263 in combination with WZ4002 to determine whether this would restore the apoptotic response. Indeed, combination treatment with ABT-263 in the two low BIM expressing clones was able to restore the apoptotic response to EGFR inhibition (data not shown).

These findings were the basis for a new clinical trial combining ABT263 with AZD9291 which as recently opened for patient accrual. Our data was presented to a national committee of lung cancer experts convened by NCI-CTEP and was chosen from several potential ideas as a promising concept. A clinical trial proposal was designed by these experts (including Dr. Engelman) and presented to the NCI Investigational Drug Steering Committee, who voted to proceed with the trial. Hence, a national CTEP-

sponsored trial is now enrolling, directly based on our findings and immediately as a result of the studies supported by this DOD award.

4.KEY RESEARCH ACCOMPLISHMENTS:

- During this award, we have continued to surpass our initial goals of obtaining pre-treatment and post-treatment biopsy specimens for both *EGFR* mutant and *ALK*-translocated tumors.
- We have successfully optimized our methods to establish cell lines taken from patient-derived tumors taken at the time of progression. This has allowed us to expand the number of both *in vitro* and xenograft models for laboratory use. (published in *Science*).
- Intrinsic loss of apoptotic response appears to be a distinct mechanism contributing to acquired resistance and not mutually exclusive with commonly clinically observed genetic clinical mechanisms of resistance such as T790M (published in *Nature Medicine*).
- Cancers that evolve from drug tolerant persisters likely maintain an apoptotic defect when they subsequently acquire genetic mutations leading to resistance (published in *Nature Medicine*).
- Cancers with T790M and suppression of apoptotic response may be less sensitive to subsequent therapy with next generation irreversible EGFR inhibitors (published in *Nature Medicine*)
- Mesenchymal EGFR mutant lung cancers are resistant to EGFR inhibitor-induced apoptosis via insufficient expression of BIM, preventing cell death even when EGFR inhibitors potently suppresses downstream signaling (manuscript under review)
- There is a ZEB1-BIM interaction that mediates low BIM expression in NSCLCs that undergo EMT, thus revealing commonality between the two modes of resistance (manuscript under review)
- Cancers with loss of apoptotic response can be resensitized to TKI treatment by use of BH3 mimetics (published in *Nature Medicine*)
- **A new clinical trial combining ABT263 with AZD9291 has opened based on these results**

5.CONCLUSION:

We have established that a subset of resistant cancers that developed T790M have decreased apoptotic response to irreversible EGFR inhibitors *in vitro* and *in vivo*. The changes in these cells that underlie the loss of apoptotic response involves loss of/downregulation of BIM, which via ZEB1 is also linked to EMT. Though ZEB1 is not a druggable target, we have determined that the combination of BH3 mimetics plus irreversible EGFR inhibitors is effective against many of these cancers in preclinical

studies. These data have provided rationale for the now open NCI CTEP-sponsored clinical trial investigating the combination of navitoclax (ABT263) with irreversible EGFR inhibitors.

6.PUBLICATIONS, ABSTRACTS, AND PRESENTATIONS:

Two manuscripts describing the data generated by this grant have been written:

Hata AN, Niederst MJ, Archibald HL, Gomez-Caraballo M, Siddiqui FM, Mulvey HE, Maruvka YE, Ji F, Bhang HE, Krishnamurthy Radhakrishna V, Siravegna G, Hu H, Raoof S, Lockerman E, Kalsy A, Lee D, Keating CL, Ruddy DA, Damon LJ, Crystal AS, Costa C, Piotrowska Z, Bardelli A, Iafrate AJ, Sadreyev RI, Stegmeier F, Getz G, Sequist LV, Faber AC, Engelman JA. Tumor cells can follow distinct evolutionary paths to become resistant to epidermal growth factor receptor inhibition. *Nat Med*, 2016, 22(3):262-9. PMCID: PMC4900892

Niederst MJ, Lochmann TL , Song K, Hata AN, Kitai H, Ham J, Floros KV, Hu H, Mulvey HE, Drier Y, Heisey DAR, Hughes MT, Patel NU, Lockerman EL, Garcia A, Gillepsie S, Moore L, Archibald HL, Gomez-Caraballo M , Nulton TJ, Windle BE, Piotrowska Z, Sahingur SE, Taylor SM, Dozmorov M, Sequist LV, Bernstein B, Ebi H, Engelman JA, Faber AC. Epithelial-to-mesenchymal transition antagonizes response to targeted therapies in lung cancer by suppressing BIM. *Under review*.

7.INVENTIONS, PATENTS AND LICENSES: Nothing to Report

8.REPORTABLE OUTCOMES:

Two manuscripts describing the combination of ABT263 and irreversible EGFR inhibitors have been written. One was published in *Nature Medicine* and one is under review. These data are the basis of an ongoing clinical trial

9.OTHER ACHIEVEMENTS: Nothing to Report

10.REFERENCES: Nothing to Report

nature medicine

Tumor cells can follow distinct evolutionary paths to become resistant to epidermal growth factor receptor inhibition

Aaron N Hata[1,2,14], Matthew J Niederst[1,2,14], Hannah L Archibald[1], Maria Gomez-Caraballo[1], Faria M Siddiqui[1], Hillary E Mulvey[1], Yosef E Maruvka[1,3], Fei Ji[4], Hyo-eun C Bhang[5], Viveksagar Krishnamurthy Radhakrishna[5], Giulia Siravegna[6,7], Haichuan Hu[1], Sana Raoof[1,2], Elizabeth Lockerman[1], Anuj Kalsy[1], Dana Lee[1], Celina L Keating[5], David A Ruddy[8], Leah J Damon[1], Adam S Crystal[1,13], Carlotta Costa[1,2], Zofia Piotrowska[1,2], Alberto Bardelli[6,7], Anthony J Iafrate[9], Ruslan I Sadreyev[4,9], Frank Stegmeier[5], Gad Getz[1,3,9,10], Lecia V Sequist[1,2], Anthony C Faber[11,12] & Jeffrey A Engelman[1,2]

Although mechanisms of acquired resistance of epidermal growth factor receptor (EGFR)-mutant non-small-cell lung cancers to EGFR inhibitors have been identified, little is known about how resistant clones evolve during drug therapy. Here we observe that acquired resistance caused by the *EGFR*^{T790M} gatekeeper mutation can occur either by selection of pre-existing *EGFR*^{T790M}-positive clones or via genetic evolution of initially *EGFR*^{T790M}-negative drug-tolerant cells. The path to resistance impacts the biology of the resistant clone, as those that evolved from drug-tolerant cells had a diminished apoptotic response to third-generation EGFR inhibitors that target EGFR^{T790M}; treatment with navitoclax, an inhibitor of the anti-apoptotic factors BCL-xL and BCL-2 restored sensitivity. We corroborated these findings using cultures derived directly from EGFR inhibitor–resistant patient tumors. These findings provide evidence that clinically relevant drug-resistant cancer cells can both pre-exist and evolve from drug-tolerant cells, and they point to therapeutic opportunities to prevent or overcome resistance in the clinic.

Despite the success of targeted cancer therapies, the duration of clinical response is limited by the inevitable development of acquired drug resistance, as in the case of *EGFR*-mutated non-small-cell lung cancers (NSCLCs) treated with EGFR inhibitor therapy[1–3]. Although molecular mechanisms of acquired resistance to EGFR inhibitors have been identified[4–6], little is known about how resistant clones evolve during drug therapy. In some cases, clones with clinically validated genetic resistance mechanisms may exist before drug exposure and may be selected for by treatment[7–10]. Alternatively, it has been hypothesized that drug-tolerant (or 'persister') cells without bona fide resistance mechanisms may survive initial drug treatment by epigenetic adaptations[11–13] and undergo further evolution over time to acquire validated genetic resistance mechanisms (**Supplementary Fig. 1**). Although this would have immediate implications for new therapeutic strategies to prevent resistance, there has not been any direct evidence that drug-tolerant cells can undergo such an evolution.

To better understand the evolution of acquired resistance, we studied the development of resistance caused by the *EGFR*^{T790M} gatekeeper mutation, which occurs in 50–60% of individuals with EGFR-mutant NSCLC who have acquired resistance to EGFR inhibitor therapy[4]. By monitoring the development of large numbers of resistant clones in parallel, we were able to identify temporal patterns that reflected the emergence of pre-existing drug-resistant *EGFR*^{T790M}-positive clones (hereafter referred to as *EGFR*^{T790M} clones) well as the *de novo* acquisition of the *EGFR*^{T790M} mutation within initially *EGFR*^{T790M}-negative drug-tolerant cells. Moreover, clones that evolved from drug-tolerant cells had epigenetic hallmarks of the drug-tolerant state and a diminished apoptotic response to third-generation EGFR inhibitors that target EGFR^{T790M}. These findings provide evidence that drug-resistant cancer cells bearing the identical clinically relevant genetic resistance mechanism can both pre-exist and evolve from drug-tolerant cells, suggesting that cancer cells that survive initial therapy may serve as an important reservoir from which acquired resistance can emerge in the clinic.

RESULTS

Differential response of PC9-*EGFR*^{T790M} cells to EGFR inhibition

We previously cultured *EGFR*-mutated NSCLC PC9 cells in escalating concentrations of the EGFR inhibitor gefitinib until resistant clones

[1]Massachusetts General Hospital (MGH) Cancer Center, Charlestown, Massachusetts, USA. [2]Department of Medicine, Harvard Medical School, Boston, Massachusetts, USA. [3]Broad Institute of the Massachusetts Institute of Technology (MIT) and Harvard University, Cambridge, Massachusetts, USA. [4]Department of Molecular Biology, Massachusetts General Hospital, Boston, Massachusetts, USA. [5]Oncology Disease Area, Novartis Institutes for Biomedical Research, Cambridge, Massachusetts, USA. [6]Department of Oncology, University of Torino, Torino, Italy. [7]Candiolo Cancer Institute–Fondazione Piemontese per l'Oncologia (FPO), Istituto di Ricovero e Cura a Carattere Scientifico (IRCCS), Candiolo, Italy. [8]Translational Clinical Oncology, Novartis Institutes for Biomedical Research, Cambridge, Massachusetts, USA. [9]Department of Pathology, Massachusetts General Hospital, Boston, Massachusetts, USA. [10]Department of Pathology, Harvard Medical School, Boston, Massachusetts, USA. [11]Virginia Commonwealth University Philips Institute for Oral Health Research, Virginia Commonwealth University School of Dentistry, Richmond, Virginia, USA. [12]Virginia Commonwealth University Massey Cancer Center, Richmond, Virginia, USA. [13]Present address: Translational Clinical Oncology, Novartis Institutes for Biomedical Research, Cambridge, Massachusetts, USA. [14]These authors contributed equally to this work. Correspondence should be addressed to J.A.E. (jengelman@partners.org).

Received 4 August 2015; accepted 28 December 2015; published online 1 February 2016; doi:10.1038/nm.4040

emerged[14]. In two resistant cell lines that acquired the *EGFR*^{T790M} mutation, there was a marked difference in the time required to develop resistance, with the PC9-GR2 and PC9-GR3 lines developing in 6 and 24 weeks, respectively (**Fig. 1a**). Treatment with the third-generation irreversible EGFR inhibitor WZ4002 (ref. 15) suppressed EGFR phosphorylation and downstream mitogen-activated protein kinase (MAPK) kinase (MEK) and phosphatidylinositol-4,5-bisphosphate 3-kinase (PI3K) signaling, and it induced cell cycle arrest in both resistant cell lines (**Supplementary Fig. 2a–c**). However, WZ4002 treatment induced more robust mitochondrial depolarization and subsequent apoptosis in the PC9-GR2 cells than in the PC9-GR3 cells (**Fig. 1b** and **Supplementary Fig. 2d**). Analysis of the expression of *BCL2* family genes, whose products regulate the mitochondrial apoptotic response induced by the MEK and extracellular signal–regulated kinase (ERK) and the PI3K and protein kinase B (AKT) signaling pathways[16] revealed that, as compared to parental and PC9-GR2 cells, PC9-GR3 cells had diminished upregulation of BIM (**Supplementary Fig. 2e**,**f**), a key mediator of apoptosis in EGFR-mutant NSCLC[17–20]. Similarly, induction of BIM protein levels after drug treatment was significantly lower ($P < 0.05$) in PC9-GR3 cells than in PC9-GR2 or parental cells (**Supplementary Fig. 2a**,**g**). Consistent with the differential levels of apoptosis observed after treatment with WZ4002, a cytotoxic response in PC9-GR2 but not PC9-GR3 cells was induced *in vitro* after treatment with WZ4002 (**Fig. 1c** and **Supplementary Fig. 2h**). *In vivo*, WZ4002 treatment suppressed the growth of subcutaneous PC9-GR3 xenograft tumors, but it did not induce tumor regression to the degree observed for PC9-GR2 tumors (**Fig. 1d**), despite comparable inhibition of EGFR and ERK phosphorylation (**Supplementary Fig. 3a**).

Early-resistant clones derive from pre-existing *EGFR*^{T790M}-containing cells

The variable time to resistance led us to question whether the PC9-GR2 and PC9-GR3 cells may have developed the *EGFR*^{T790M} mutation via different mechanisms (i.e., pre-existing mutation versus drug-tolerant evolution (**Supplementary Fig. 1**)). To explore this possibility, we cultured over 1,200 small pools (5,000 cells each) of parental PC9 cells in the presence of gefitinib and monitored them for the emergence of resistant clones. After 2 weeks of drug exposure, 5–10% of the wells contained a rapidly growing, resistant colony (**Fig. 2a**), whereas the other wells contained a small number of surviving, drug-tolerant cells similar to those described previously by Settleman and colleagues[11]. Allele-specific quantitative PCR revealed that all 'early-resistant' colonies examined ($n = 50$) harbored the *EGFR*^{T790M} mutation (**Supplementary Fig. 4a**) and that all of the colonies were sensitive to WZ4002 but not to gefitinib (**Fig. 2b**). In contrast, treatment of PC9 pools with WZ4002 treatment for 2 weeks yielded drug-tolerant cells but completely suppressed emergence of the early *EGFR*^{T790M} colonies (**Fig. 2c**). Conversely, treatment of PC9 pools with gefitinib and the insulin-like growth factor (IGF)-1 receptor (IGF-1R) inhibitor AEW541, which was previously shown to abrogate the survival of drug-tolerant PC9 cells[11], eliminated the drug-tolerant cells without affecting the emergence of early-resistant *EGFR*^{T790M} clones. These results demonstrate that the early-resistant *EGFR*^{T790M} clones emerged independently from drug-tolerant cells.

We hypothesized that the early-resistant *EGFR*^{T790M} clones derived from rare pre-existing *EGFR*^{T790M}-containing cells that existed in our parental PC9 cell line. Direct detection of genetically distinct rare subpopulations using currently available standard next-generation sequencing (NGS) is limited to allelic frequencies of ~0.1% (ref. 21), whereas droplet digital PCR (ddPCR) has a sensitivity of 0.01–0.005% (ref. 22). In our parental PC9 cell line, we estimated that ~1 out of 25,000–50,000 cells harbor an *EGFR*^{T790M} allele before treatment (see Online Methods for calculation). Because PC9 cells carry 8–10 copies of *EGFR* (**Supplementary Fig. 4b**) and only one *EGFR*^{T790M} allele is required to confer resistance (**Supplementary Fig. 4c**,**d**), direct detection of the pre-existing *EGFR*^{T790M} clones in our parental PC9 population would necessitate a sensitivity at least an order of magnitude beyond what is routinely achievable.

To overcome these limitations, we used a recently reported high-complexity DNA barcode library (ClonTracer) designed to track the evolution of pre-existing resistant clones too rare to be detected by NGS or ddPCR[8]. In this system, when a population of barcoded cells is made resistant to drug, enrichment of a shared set of barcodes between multiple replicates indicates selection of pre-existing resistant clones. We transduced ~1×10^6 to 2×10^6 PC9 cells with lentiviral ClonTracer barcodes, expanded the culture and split it (we refer to this population

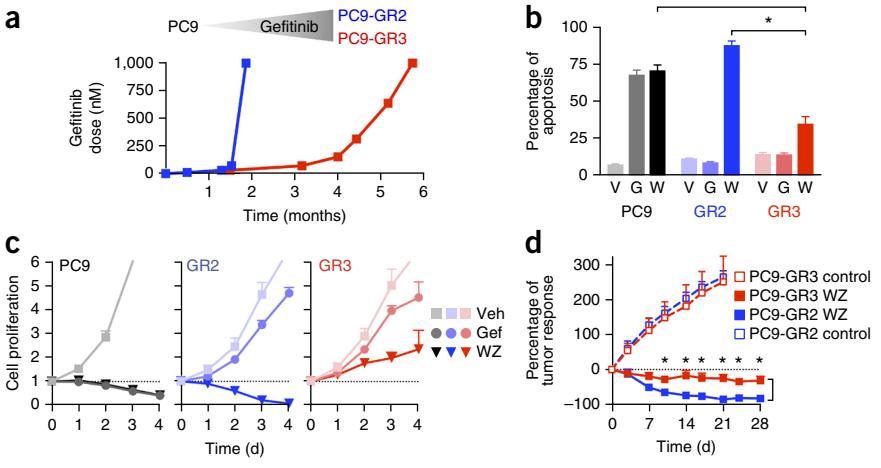

Figure 1 Variable sensitivity of gefitinib-resistant *EGFR*^{T790M}-positive PC9 cell lines to EGFR inhibition. (**a**) Development of PC9-GR2 (blue) and PC9-GR3 (red) gefitinib-resistant cell lines after culturing parental PC9 cells in escalating concentrations of gefitinib. (**b**) Apoptosis, as determined by annexin V staining, of parental PC9, PC9-GR2 (GR2) and PC9-GR3 (GR3) after treatment with vehicle (V) or with 1 μM gefitinib (G) or WZ4002 (W) for 72 h. Data are mean ± s.e.m. of four independent experiments. *$P < 0.05$; two-tailed Student's *t*-test. (**c**) Proliferation of parental PC9 (left), PC9-GR2 (middle) and PC9-GR3 (right) cells, as determined by CellTiter-Glo assays at the indicated time points, after treatment with vehicle (Veh) or with 1 μM gefitinib (Gef) or WZ4002 (WZ). Data are mean ± s.e.m. of four independent experiments. The dotted line indicates the relative cell number at the time of drug addition. (**d**) Change in tumor volume (relative to start of drug treatment), represented as percentage of tumor response, in mice with PC9-GR2– or PC9-GR3–derived subcutaneous xenograft tumors that were treated with WZ4002 (50 mg per kg body weight per day (mg/kg/d)) or left untreated (control) ($n = 8$ mice per group). Data are mean ± s.e.m. *$P < 0.01$; by comparing the WZ-treatment arms at the indicated time points by multiple *t*-tests with Sidak-Bonferroni correction for multiple comparisons.

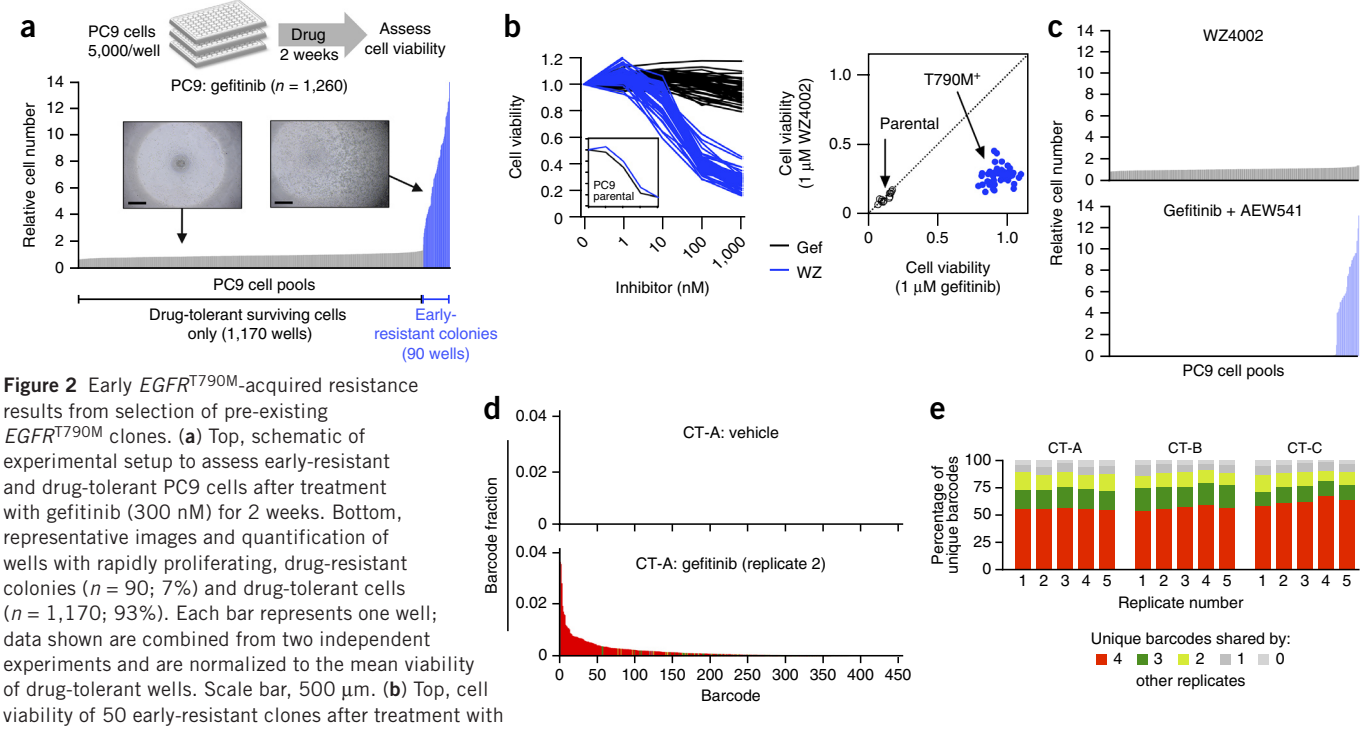

Figure 2 Early *EGFR*^{T790M}-acquired resistance results from selection of pre-existing *EGFR*^{T790M} clones. (**a**) Top, schematic of experimental setup to assess early-resistant and drug-tolerant PC9 cells after treatment with gefitinib (300 nM) for 2 weeks. Bottom, representative images and quantification of wells with rapidly proliferating, drug-resistant colonies (n = 90; 7%) and drug-tolerant cells (n = 1,170; 93%). Each bar represents one well; data shown are combined from two independent experiments and are normalized to the mean viability of drug-tolerant wells. Scale bar, 500 μm. (**b**) Top, cell viability of 50 early-resistant clones after treatment with gefitinib (Gef) or WZ4002 (WZ) for 72 h. Inset shows dose response of parental PC9 cells. Bottom, cell viability of each early-resistant *EGFR*^{T790M} clone (T790M+) after treatment with 1 μM WZ4002 or gefitinib, relative to that of vehicle control. Diagonal axis indicates equal sensitivity to both drugs (such as clones lacking the *EGFR*^{T790M} mutation), whereas sensitivity to WZ4002 but not to gefitinib indicates *EGFR*^{T790M} clones (blue circles). Parental cells, which are sensitive to both drugs, are shown for comparison. (**c**) Cell viability of PC9 cell pools (5,000 cells) after treatment with 1 μM WZ4002 (top; n = 420) or 300 nM gefitinib + 500 nM AEW541 (bottom; n = 420) for 2 weeks. (**d**) Barcode distribution (fraction of each unique barcode in the total barcode reads) of one representative replicate of ClonTracer-barcoded PC9 cells (CT-A) after treatment with vehicle (top) or gefitinib (bottom). The x axes of the histograms are identical; each bar represents one unique barcode. Colors denote the number of other replicates in which the barcodes were identified, as defined in **Figure 2e**. (**e**) Percentage of enriched barcodes shared by each replicate (1–5) for each independently barcoded experiment (CT-A, CT-B and CT-C). Colored key denotes barcodes shared by four (red), three (dark green), two (light green), one (dark gray) or no (light gray) other replicates.

of cells as replicate group CT-A) into multiple biological replicates of 20×10^6 cells each to ensure tenfold representation of barcode complexity (**Supplementary Fig. 5a**). We treated the cells with 300 nM gefitinib and, consistent with our prior experiments, observed rapidly proliferating early-resistant clones at 2–3 weeks. These clones were *EGFR*^{T790M} positive (**Supplementary Fig. 5b**), and we observed a consistent number of unique barcodes enriched in each replicate (**Fig. 2d** and **Supplementary Fig. 5c**). Approximately 90% of enriched barcodes in each sample were shared by at least two other replicates, and over 50% of the barcodes were shared by all five replicates (**Fig. 2e** and **Supplementary Fig. 5d**). Notably, the most highly shared barcodes were also the most highly enriched. We repeated the entire experiment with two additional, independently barcoded PC9 populations (CT-B and CT-C) and found the same results (**Fig. 2e** and **Supplementary Fig. 5b–d**). These results confirm that the early-resistant *EGFR*^{T790M} clones were derived from pre-existing *EGFR*^{T790M}-mutated cells that were selected for during the gefitinib treatment.

Late-emerging *EGFR*^{T790M} clones derive from drug-tolerant cells

To determine whether the *EGFR*^{T790M} allele could also evolve from initially *EGFR*^{T790M}-negative drug-tolerant cells during drug treatment, we cultured 16 drug-tolerant PC9 cell pools that showed no evidence of early-resistant clones in the continuous presence of gefitinib until they had reached numbers sufficient for genotyping and drug-sensitivity testing, which required 12–16 weeks. These pools—which we refer to as 'intermediate-resistant'—remained partially resistant to both gefitinib and WZ4002, and allele-specific PCR for *EGFR*^{T790M} was negative, indicating non–*EGFR*^{T790M}-mediated resistance (**Fig. 3a** and **Supplementary Fig. 6a**). These cells were further cultured in gefitinib until they became fully resistant, and 5 of 16 resistant pools acquired the *EGFR*^{T790M} mutation and demonstrated increased sensitivity to WZ4002 than to gefitinib (**Fig. 3a** and **Supplementary Fig. 6b**). To gain a better understanding of the kinetics of evolution of *EGFR*^{T790M}-mediated resistance in these cells, we examined additional intermediate time points during the development of the original PC9-GR3 resistant line and several of the late-emerging *EGFR*^{T790M} clones. For the PC9-GR3 line, the *EGFR*^{T790M} mutation was first detected at 22 weeks, at a fraction of 6% of the total cell population, and within 1 month these cells had overtaken the population as the dominant clone (**Supplementary Figs. 4d** and **6c**,**d**). For three late-emerging *EGFR*^{T790M} clones that we examined, a minority *EGFR*^{T790M} clone was observed at 34, 43 and 47 weeks, respectively, and by 1 month later it had overtaken the population (**Supplementary Fig. 6d**). Thus, these results suggest that the *EGFR*^{T790M} resistance mutation can develop *de novo* in drug-tolerant cells during the course of prolonged exposure to an EGFR inhibitor.

We subjected resistant cells that remained *EGFR*^{T790M} negative to a clinical genotyping assay that detects single-nucleotide variants (SNVs) and insertions and deletions (indels) in 39 cancer-related genes[23]. Notably, these *EGFR*^{T790M}-negative resistant cells had mutations in the oncogenes *NRAS*, *KRAS*, *BRAF* and *RET* (**Supplementary Fig. 7a**), although at low allele frequencies, suggesting mixed clonal

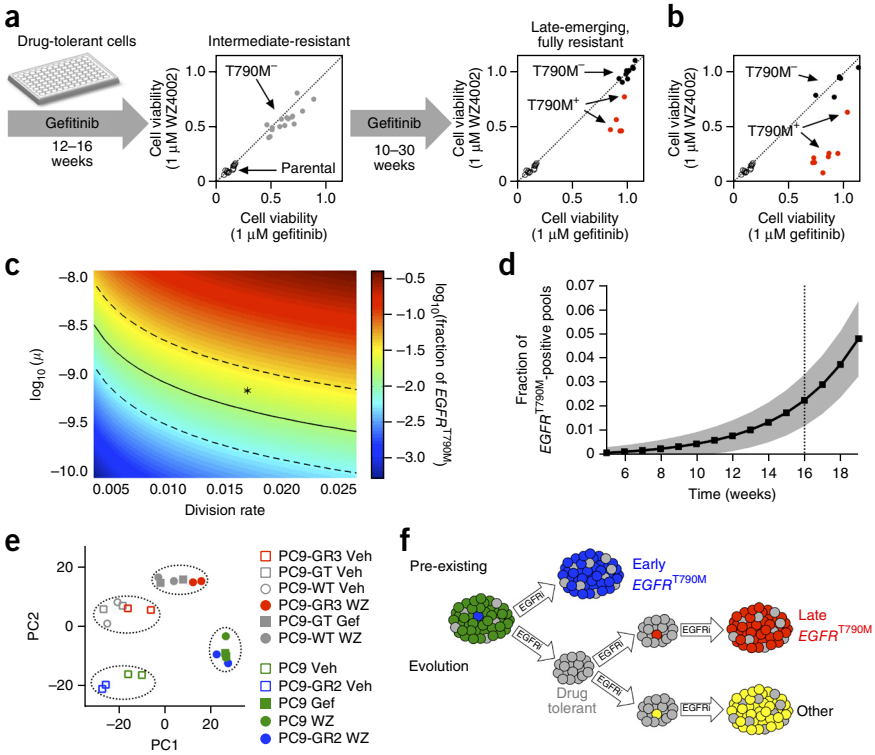

Figure 3 Late-emerging *EGFR*^{T790M}-acquired resistance results from evolution of drug-tolerant cells. (**a**) Schematic and graphs showing the presence of intermediate-resistant and late-emerging gefitinib-resistant PC9 cells that either do not have (T790M^{-}) or have (T790M^{+}) the *EGFR*^{T790M} mutation (see also **Supplementary Fig. 6a**,**b**). (**b**) *EGFR*^{T790M} status of pools of PC9 single-cell–derived subclone A cells after treatment with gefitinib until the cells were fully drug resistant (see also **Supplementary Fig. 7b**). (**c**) The frequency of PC9 drug-tolerant cell pools developing an *EGFR*^{T790M} mutation during 16 weeks of drug treatment, mathematically modeled as a function of varying mutational rates (μ) and cell division rates. Frequency values were calculated from the analytical solution of the mathematical model and are depicted as $\log_{10}$ of the fraction of wells predicted to develop cells with the *EGFR*^{T790M} mutation. Parameters that yield the experimentally observed frequency of 1.5% are indicated by the solid (mean) and dashed (95% confidence interval) lines. The asterisk (*) denotes parameters used in **Figure 3d**. The range of the *x* axis corresponds to a division rate of once every 2 weeks (left) to the rate of PC9 cells in the absence of drug (right). (**d**) Predicted frequency of acquiring the *EGFR*^{T790M} mutation as a function of time. Data are represented as mean (black line) ± s.d. (gray shading). Parameters used for drug-tolerant cells: initial population size $N_0 = 150$; birth rate $b = 0.0162$; death rate $d = 0.015$; mutation rate $\mu = 7 \times 10^{-10}$. Birth and death rates of *EGFR*^{T790M}-positive cells are $b_r = 0.04$ and $d_r = 0.0015$, respectively. (**e**) PCA of transcriptional profiles of parental PC9, drug-tolerant (selected for 2 weeks in the presence of gefitinib (GT) or WZ4002 (WZ)), early-resistant PC9-GR2 *EGFR*^{T790M}-positive and late-resistant PC9-GR3 *EGFR*^{T790M}-positive cells, as determined by RNA-seq analysis. Prior to harvesting RNA, cells were treated with vehicle (Veh) or with 1 μM gefitinib (Gef) or WZ4002 (WZ) for 24 h. (**f**) Model for the development of *EGFR*^{T790M}-acquired resistance from either pre-existing *EGFR*^{T790M} cells or from the evolution of initially *EGFR*^{T790M}-negative drug-tolerant cells. EGFRi denotes EGFR inhibitor treatment, such as that with gefitinib.

populations. We did not observe amplification of the *MET* or *ERBB2* (also known as *HER2*) oncogene, and one resistant line had low-level amplification (**Supplementary Fig. 7b**) in *KRAS* in addition to a *KRAS* mutation. Although some of these mutations have been previously observed in PC9 cells and in resistant EGFR-mutant NSCLC tumors[24,25], the significance of these particular mutations in driving resistance in the clinic is unclear. Of note, the gefitinib-resistant *EGFR*^{T790M}-negative PC9-GR1 cell line developed in parallel with the PC9-GR2 and PC9-GR3 lines that we previously reported to be sensitive to the combined inhibition of EGFR and MEK[14] developed at a rate nearly identical to that of the drug-tolerant–derived *EGFR*^{T790M}-positive PC9-GR3 cell line (**Supplementary Fig. 7c**). Taken together, these results suggest that drug-tolerant cells have the potential to develop both *EGFR*^{T790M}-dependent and *EGFR*^{T790M}-independent mechanisms of resistance, which may contribute to the heterogeneity of acquired resistance observed in the clinic[4,26].

To further demonstrate that *EGFR*^{T790M} could evolve during treatment from initially *EGFR*^{T790M}-negative drug-tolerant cells, we established PC9 subclone lines derived from single cells to eliminate pre-existing *EGFR*^{T790M}-containing cells. Indeed, in ten independent single-cell subclone lines, no early *EGFR*^{T790M} colonies emerged after 2 weeks of gefitinib treatment (**Supplementary Fig. 8a**), in contrast to the parental PC9 cells which harbored pre-existing *EGFR*^{T790M} cells (**Fig. 2a**). We then cultured 14 pools (5,000 cells each) from single-cell subclone A (**Supplementary Fig. 8a**) in gefitinib for up to 40 weeks, until fully resistant cells emerged. Eight pools acquired the *EGFR*^{T790M} mutation, and six pools remained *EGFR*^{T790M} negative (**Fig. 3b** and **Supplementary Fig. 8b**). Similarly, three additional single-cell subclones (B, C and D) were cultured in gefitinib for several months, and all developed late-resistant *EGFR*^{T790M} clones (data not shown). To provide statistical evidence that these late-emerging *EGFR*^{T790M} clones did not derive from undetected pre-existing *EGFR*^{T790M} cells, we spiked single RFP-labeled *EGFR*^{T790M} PC9 cells into pools of unlabeled subclone A, subclone B, subclone C and subclone D (5,000 cells each) and measured the kinetics of emergence of resistant cells. Over a 10-week time period, all resistant clones were derived from RFP-positive *EGFR*^{T790M} cells, with the majority emerging within the first 2 weeks (**Supplementary Fig. 8c**). From this, we derived a cumulative density function (CDF) describing the probability of detecting the emergence of pre-existing resistant *EGFR*^{T790M} cells as a function of time (**Supplementary Fig. 8d**,**e**). Because none of the single cell–derived subclones (A–D) gave rise to early-resistant *EGFR*^{T790M} clones at 2 weeks (**Supplementary Fig. 8a**), the CDF determined that the probability that the late-resistant *EGFR*^{T790M} clones that eventually emerged were derived from undetected pre-existing *EGFR*^{T790M} cells is 0.006 (see legend of **Supplementary Fig. 8** for calculation). Taken together, these results confirm that *EGFR*^{T790M}-acquired resistance can evolve from initially *EGFR*^{T790M}-negative drug-tolerant cells.

Considering the time scale and cell population sizes of our experiments, we were initially surprised that the *EGFR*^{T790M} mutation could arise in the slow-growing drug-tolerant cells. Taking into account reasonable estimates of mutation and cell division rates and the experimentally determined growth rates of drug-tolerant cells, we

mathematically modeled the *de novo* acquisition of the *EGFR*^{T790M} mutation during drug treatment (**Supplementary Fig. 9a**,**b**; see Online Methods for details) and calculated the fraction of drug-tolerant pools that are predicted to acquire the *EGFR*^{T790M} mutation during 16 weeks of gefitinib treatment for a range of mutation and division rates (**Fig. 3c**). This fraction grows linearly with the initial population size and division and mutation rates, and grows exponentially with the growth rate and time (for fractions of <10%). Using a reasonable set of parameters, the mathematical model did predict emergence of the *EGFR*^{T790M} mutation over a time period corresponding to several months (**Fig. 3d**). When we tested this model experimentally, we found that 1.5% of drug-tolerant PC9 pools developed the *EGFR*^{T790M} mutation over an equivalent time period, in agreement with the modeling results (**Supplementary Fig. 9c**).

To examine whether the *EGFR*^{T790M} mutation can evolve from drug-tolerant cells in other *EGFR*-mutated NSCLC models, we examined MGH119 cells that were previously derived in our laboratory from a treatment-naive individual with *EGFR*-mutated NSCLC[14]. MGH119 cells were cultured in gefitinib until they were drug resistant, and two independent *EGFR*^{T790M} lines (MGH119-GR1 and MGH119-GR2) developed after 5–6 months. To determine whether *EGFR*^{T790M} cells pre-exist in this model, we treated pools of MGH119 cells with gefitinib for 3 weeks but did not observe any early-resistant colonies (**Supplementary Fig. 10a**). In contrast, when we simulated the presence of pre-existing *EGFR*^{T790M}-containing cells by introducing red fluorescent protein (RFP)-labeled MGH119-GR1 cells in MGH119 parental cell cultures, we detected emerging gefitinib-resistant RFP-positive colonies after 2–3 weeks of drug treatment (**Supplementary Fig. 10b**). After 10 weeks of treatment, only RFP-positive resistant clones were observed. These results suggest that the MGH119 cell line does not harbor pre-existing *EGFR*^{T790M} cells, and that the MGH119-GR1 and MGH119-GR2 resistant cells arose from drug-tolerant cells by acquiring the *EGFR*^{T790M} mutation during the course of the drug treatment.

Late-resistant *EGFR*^{T790M} cells have hallmarks of the drug-tolerant state

We next sought to determine whether late-resistant *EGFR*^{T790M} cells exhibit molecular evidence of evolution from the drug-tolerant state. Using RNA sequencing (RNA-seq) analysis, we compared the transcriptional profiles of drug-tolerant PC9 cells with those of PC9-GR3, PC9-GR2 and parental PC9 cells (**Supplementary Fig. 11a**). Principal component analysis (PCA) of mRNA expression at baseline and after treatment with the EGFR inhibitor WZ4002 revealed that the late-resistant *EGFR*^{T790M} PC9-GR3 cells clustered with drug-tolerant cells and that the early-resistant *EGFR*^{T790M} PC9-GR2 cells clustered with the parental PC9 cells (**Fig. 3e**). Whereas principal component 1 (PC1) primarily differentiated between baseline and drug-treated samples, PC2 segregated PC9-GR3 and drug-tolerant cells from early-resistant PC9-GR2 and parental cells (**Supplementary Fig. 11b**). Gene-set enrichment analysis revealed the upregulation of genes related to epithelial-to-mesenchymal transition (EMT) in drug-tolerant and PC9-GR3 cells relative to the parental and PC9-GR2 cells; this pathway has been linked to resistance to EGFR inhibitor therapy in the clinic[4]. These results demonstrate that the late-emerging PC9-GR3 cells share a transcriptional profile most similar to that of drug-tolerant cells. This further supports the model that the late-resistant *EGFR*^{T790M} cells evolved from drug-tolerant cells (**Fig. 3f**) and suggests that molecular features of the drug-tolerant state that impact drug sensitivity may be maintained even after acquisition of the *EGFR*^{T790M} mutation.

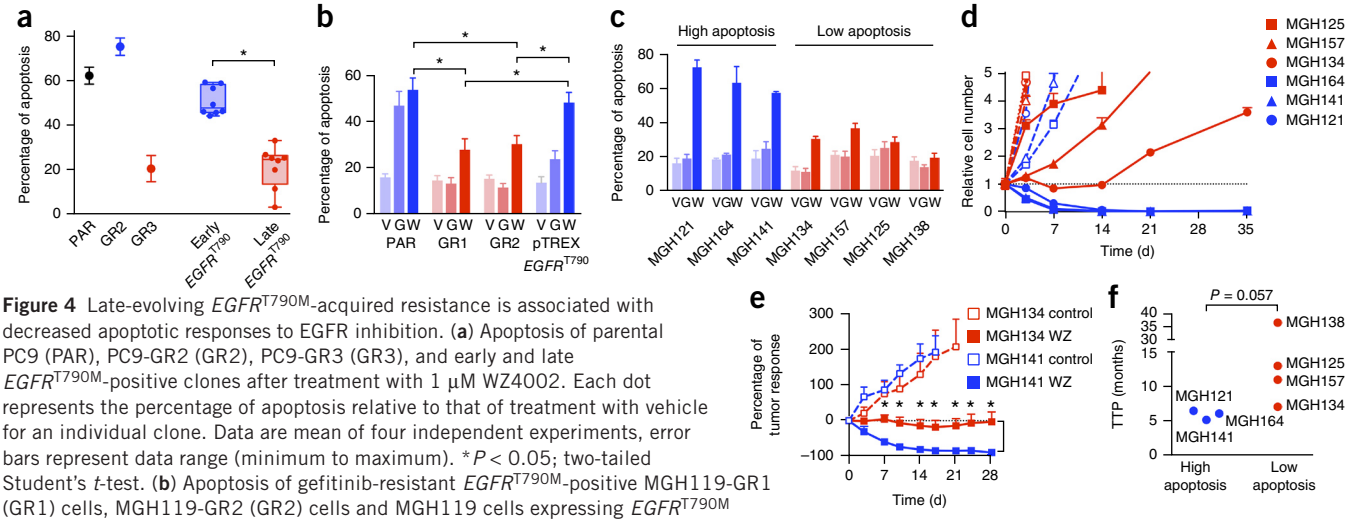

Figure 4 Late-evolving *EGFR*^{T790M}-acquired resistance is associated with decreased apoptotic responses to EGFR inhibition. (**a**) Apoptosis of parental PC9 (PAR), PC9-GR2 (GR2), PC9-GR3 (GR3), and early and late *EGFR*^{T790M}-positive clones after treatment with 1 μM WZ4002. Each dot represents the percentage of apoptosis relative to that of treatment with vehicle for an individual clone. Data are mean of four independent experiments, error bars represent data range (minimum to maximum). *$P < 0.05$; two-tailed Student's *t*-test. (**b**) Apoptosis of gefitinib-resistant *EGFR*^{T790M}-positive MGH119-GR1 (GR1) cells, MGH119-GR2 (GR2) cells and MGH119 cells expressing *EGFR*^{T790M} from a lentiviral construct (pTREX- *EGFR*^{T790M}), and of parental (PAR) MGH119 cells after treatment with vehicle (V) or with 1 μM gefitinib (G) or WZ4002 (W). Data are mean ± s.e.m. of three independent experiments. *$P < 0.05$; two-tailed Student's *t*-test. (**c**) Apoptosis of patient-derived *EGFR*^{T790M}-mutated NSCLC cell lines after treatment with gefitinib, WZ4002 or vehicle. Data are mean ± s.e.m. of four independent experiments. (**d**) Drug sensitivity of patient-derived cell lines with decreased apoptotic response after treatment with 1 μM WZ4002 (closed symbols, solid lines) or vehicle (open symbols, dashed lines), as represented by relative cell number determined by nuclear counting using high-content imaging. Data are mean ± s.e.m. of four replicates. (**e**) Change in tumor volume (relative to start of drug treatment), represented as percentage of tumor response, in mice with MGH134-derived (control, $n = 8$; WZ, $n = 10$) or MGH141-derived (control, $n = 7$; WZ, $n = 8$) subcutaneous xenograft tumors after treatment with WZ4002 (50 mg/kg/day). Data are mean ± s.e.m. *$P < 0.01$; by comparing WZ-treatment arms at the indicated time points by using multiple *t*-tests with Sidak-Bonferroni correction for multiple comparisons. (**f**) Time-to-progression (TTP) of patients from whom patient-derived *EGFR*^{T790M} cell lines were established. TTP was determined as time from initiation of first-line EGFR inhibitor therapy to first restaging scan showing definitive clinical progression of disease. Grouping of cell lines corresponds to that in **Figure 4c**. Statistical significance was calculated using the Mann-Whitney *U* test.

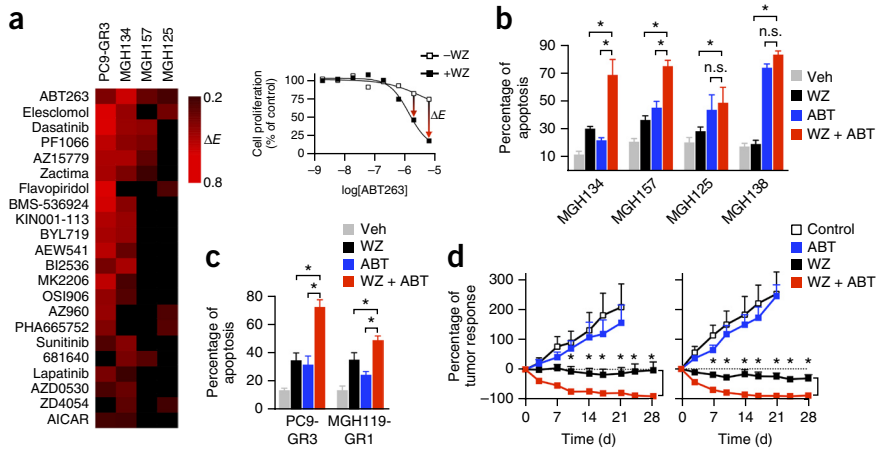

Figure 5 Navitoclax enhances the apoptotic response of late-resistant *EGFR*^{T790M} cells with decreased sensitivity to EGFR inhibition. (**a**) Left, top drug hits from a combination drug screen[14] that led to an enhancement of E_{max} when combined with WZ4002 treatment in at least two of four *EGFR*^{T790M}-positive cell lines screened. Right, the response of MGH134 cells to treatment with ABT-263 is shown as an example. (**b**) Apoptotic response of patient-derived *EGFR*^{T790M} cell lines to treatment with 1 μM WZ4002 or ABT-263, or a combination of both drugs. Data are mean ± s.e.m. of four independent experiments. *$P < 0.05$; by two-tailed Student's *t*-test; n.s., not significant. (**c**) Apoptotic response of *in vitro*–derived late-emerging, *EGFR*^{T790M}-positive, gefitinib-resistant cell lines to treatment with 1 μM WZ4002 or ABT-263, or a combination of drugs. Data are mean ± s.e.m. of four independent experiments. *$P < 0.05$; by two-tailed Student's *t*-test. (**d**) Change in tumor volume (relative to start of drug treatment), represented as percentage of tumor response, in mice with MGH134-derived (left) and PC9-GR3–derived (right) subcutaneous xenograft tumors after treatment with navitoclax (100 mg/kg/day) and/or WZ4002 (50 mg/kg/day) (mice with MGH134-derived tumors: control, $n = 8$; WZ, $n = 10$; ABT, $n = 8$; WZ + ABT, $n = 7$; mice with PC9-GR3–derived tumors: control, $n = 8$; WZ, $n = 8$; ABT, $n = 7$; WZ + ABT, $n = 7$). Control and WZ data from **Figures 1d** and **4e** are shown for comparison. Data are mean ± s.e.m. *$P < 0.01$; by comparing WZ and WZ + ABT treatment arms at indicated time points by using multiple *t*-tests with Sidak-Bonferroni correction for multiple comparisons.

Late-resistant *EGFR*^{T790M} cells have reduced apoptosis after EGFR inhibition

By definition, evasion of drug-induced apoptosis is a characteristic feature of drug-tolerant cells (**Supplementary Fig. 12**). Because late-resistant *EGFR*^{T790M} cells evolved from drug-tolerant cells and continue to share a similar mRNA expression profile as those cells (**Fig. 3e**), we reasoned that they might also exhibit reduced apoptotic sensitivity to subsequent EGFR inhibition. Similarly to PC9-GR3 cells (**Fig. 1b**), late-resistant *EGFR*^{T790M}-positive PC9 clones that emerged from drug-tolerant cells had a reduced apoptotic response to WZ4002 treatment as compared to that of early-resistant *EGFR*^{T790M} clones that were derived from pre-existing cells (**Fig. 4a**). Moreover, after we induced the expression of EGFR^{T790M} in drug-tolerant cells, the *EGFR*^{T790M} clones that grew out had reduced apoptotic sensitivity to WZ4002 (**Supplementary Fig. 13a**,**b**). MGH119-GR1 and MGH119-GR2 cells—which developed the *EGFR*^{T790M} mutation late, consistent with evolution from drug-tolerant cells—also exhibited reduced apoptotic response to WZ4002 treatment relative to that of the MGH119 parental cells and the MGH119 cells in which we introduced an *EGFR*^{T790M}-containing allele by using a lentiviral (pTREX) construct (**Fig. 4b** and **Supplementary Fig. 13c**). These results demonstrate that *EGFR*^{T790M} cells that evolve from drug-tolerant cells have reduced dependence on EGFR activation for survival as compared to cells with a pre-existing *EGFR*^{T790M} mutation. This is consistent with the notion that drug-tolerant cells are, by definition, the cells that do not undergo apoptosis after initial EGFR inhibition.

To investigate the clinical implications of the laboratory-derived acquired-resistance models, we examined cell lines derived from *EGFR*-mutated NSCLC patient tumors at the time of clinical progression due to *EGFR*^{T790M}-acquired resistance[14] (**Supplementary Table 1**). Three cells lines were exquisitely sensitive to WZ4002 treatment (MGH121, MGH164 and MGH141), whereas four had a diminished apoptotic response and increased *in vitro* survival (MGH134, MGH157, MGH125 and MGH138) (**Fig. 4c**,**d**). The *in vivo* sensitivity of MGH141- and MGH134-derived xenograft tumors to WZ4002 treatment mirrored that of the *in vitro* response—xenografts derived from the MGH134 cell line, which shows diminished apoptosis, failed to undergo tumor regression (**Fig. 4e**), despite suppression of EGFR and ERK signaling (**Supplementary Fig. 3b**). Notably, the least WZ4002-sensitive cell lines were from patients who had the longest duration of response to first-line EGFR inhibitor therapy before the development of drug resistance (**Fig. 4f**), raising the possibility that the *EGFR*^{T790M}-positive drug-resistant cells with low levels of apoptosis evolved from drug-tolerant cells.

These results suggest that drug-resistant cancers in which the *EGFR*^{T790M} mutation arises during therapy may have reduced apoptotic sensitivity to third-generation EGFR inhibitors that are currently being evaluated in the clinic[27–29]. Therefore, we sought to identify therapeutic strategies that could enhance the apoptotic response of these cells to third-generation EGFR inhibitors. Recently, we reported a drug-screening strategy to identify effective drug combinations for cancers with acquired resistance to targeted therapies[14]. Because this screen was focused on overcoming resistance caused by bypass tracks (i.e., compensatory signaling pathways that reestablish activation of key downstream proliferation and survival signals, despite inhibition of the original oncogene), effective drug combinations were identified on the basis of a shift in GI_{50} (drug concentration required to achieve 50% growth inhibition) values. However, we noted that the decrease in apoptosis in our models was most clearly reflected by a change in the E_{max} (maximum growth inhibition achieved) values (**Supplementary Fig. 14**). We therefore reanalyzed the screening data for three *EGFR*^{T790M}-positive patient-derived cell lines (MGH134, MGH157 and MGH125) to identify drugs that, in combination with WZ4002 treatment, increased E_{max} values. Additionally, we performed the identical drug screen on PC9-GR3 cells, by using WZ4002 treatment as the anchor. Of the top-scoring compounds for each cell line, the only one common to all four was the dual BCL-xL and BCL-2 inhibitor ABT-263 (also called navitoclax) (**Fig. 5a**). Notably, prior laboratory studies have demonstrated that dual BCL-xL and BCL-2 inhibitors can enhance the apoptotic activity of targeted therapies that induce apoptosis by inducing the expression of BIM[17,30,31], presumably by decreasing the capacity of BCL-xL to neutralize BIM. Treatment with the combination of WZ4002 and navitoclax induced significantly more apoptosis as compared to treatment with WZ4002 alone in both *EGFR*^{T790M}-positive patient-derived

cell lines that have low levels of WZ4002-induced apoptosis (**Fig. 5b**) and *in vitro*–generated drug-resistant *EGFR*^{T790M} cell lines (**Fig. 5c**. Combined treatment with WZ4002 and navitoclax also induced regression of MGH134- or PC9-GR3–derived xenograft tumors in mice (**Fig. 5d**). Thus, combining navitoclax with third-generation EGFR inhibitors may be an effective strategy for treating *EGFR*^{T790M}-positive cancers that have a decreased apoptotic response to EGFR inhibition. Indeed, an upcoming clinical trial will examine the effect of using the combination of AZD9291 and navitoclax to treat *EGFR*-mutated NSCLC with acquired resistance to first-line EGFR inhibitors (ClinicalTrials.gov study NCT02520778).

DISCUSSION

It is now well appreciated that substantial genetic heterogeneity exists between cancer cell clones within a tumor[32,33]. Pre-existing intratumoral heterogeneity has been shown to influence treatment response and the development of acquired resistance to targeted therapy in some contexts[34], but there has been little direct clinical evidence to support either emergence of pre-existing resistant clones or *de novo* evolution as the predominant mechanism of acquired resistance in lung cancer. Several studies have reported the detection of low-frequency *EGFR*^{T790M}-positive clones in clinical specimens from patients who had not started treatment yet[9,35], although doubts have been raised as to whether the majority of these may be sequencing artifacts related to tissue fixation[10].

Our results provide a proof of principle that *EGFR*^{T790M}-positive clones not only emerge from the selection of pre-existing clones but that they also can emerge from initially *EGFR*^{T790M}-negative drug-tolerant cells. Survival of drug-tolerant cancer cells may be facilitated by cell autonomous features such as altered epigenetic states[11,36] and feedback activation of alternate survival pathways[12], as well as by external stimuli from the microenvironment[13,37]. Although these mechanisms may be sufficient to prevent apoptosis and promote survival of drug-tolerant cells, they may not fully recapitulate the optimal oncogenic signaling provided by EGFR. Subsequent acquisition of the *EGFR*^{T790M} mutation probably provides an additional fitness advantage in the presence of the drug. Thus, drug-tolerant cells that are capable of surviving initial drug therapy may provide a reservoir of cells from which genetic mechanisms of acquired resistance can evolve. Consistent with our results, Altschuler and colleagues similarly observed that multiple resistant mechanisms, including that involving *EGFR*^{T790M}, can develop over time in drug-tolerant cells[38]. Such resistant clones may continue to share molecular features of the drug-tolerant cells (**Fig. 3e**,**f**), leading to a diminished apoptotic response to subsequent therapies. Our finding—that *EGFR*^{T790M}-positive cell lines derived from tumors of patients who had experienced prolonged responses to first-generation EGFR inhibitors had decreased apoptotic responses to third-generation EGFR inhibitors—suggests that tumors in which the *EGFR*^{T790M} allele arises during the course of therapy may be less responsive to third-generation EGFR inhibitors (such as AZD9291 and CO-1686)[27,28] in the clinic. However, given the limited number of patient-derived cell lines available for this study, this hypothesis warrants further investigation with additional laboratory models and validation with clinical response data.

We believe that these findings have important clinical implications. These results provide a rationale for the investigation of novel therapeutic strategies to target drug-tolerant cells, before they acquire genetic mechanisms of resistance, to prevent or delay the evolution of acquired resistance. We speculate that the majority of cancer cells that initially survive after therapy probably do not have bona fide drug-resistance mechanisms (such as *EGFR*^{T790M}-positive tumors) but more closely resemble a drug-tolerant state. Moreover, in light of recent reports that some EGFR^{T790M}-mutant NSCLCs 'lose' the *EGFR*^{T790M} mutation after developing resistance to AZD9291 or CO-1686 treatment[26,39], our studies raise the possibility that *EGFR*^{T790M}-negative drug-tolerant cells may persist in patients with drug-resistant *EGFR*^{T790M}-positive tumors and that they undergo further evolution to acquire resistance to subsequent therapies. Because we now know that these drug-tolerant cells can develop genetic mechanisms of drug resistance over time, we believe that it is imperative to develop therapeutic approaches that eliminate this reservoir of drug-tolerant cells that fail to undergo apoptosis. Such treatment strategies will also need to integrate approaches that target the rare pre-existing bona fide drug-resistant clones. We are hopeful that innovative approaches such as these will lead to more complete clinical remissions and improved patient outcomes.

METHODS

Methods and any associated references are available in the online version of the paper.

Accession codes. Gene Expression Omnibus: RNA-seq datasets from parental PC9, drug-tolerant and drug-resistant populations are available through accession number GSE75602.

Note: Any Supplementary Information and Source Data files are available in the online version of the paper.

ACKNOWLEDGMENTS

We thank C. Benes and all members of the Engelman and Benes laboratories for helpful discussions and feedback. This study was funded by support from the US National Institutes of Health (NIH) (grant R01CA137008; J.A.E.), the Department of Defense (L.V.S. and J.A.E.), LunGevity (L.V.S. and J.A.E.), Uniting Against Lung Cancer (A.N.H. and M.J.N.), the Conquer Cancer Foundation of the American Society of Clinical Oncology (A.N.H.), the Lung Cancer Research Foundation (M.J.N.), Targeting a Cure for Lung Cancer (J.A.E.), Be a Piece of the Solution (J.A.E.), and the John and Carol Barry Foundation (A.N.H.).

AUTHOR CONTRIBUTIONS

A.N.H., M.J.N. and J.A.E. designed the study, analyzed the data and wrote the paper. A.N.H., M.J.N., H.L.A., M.G.-C., F.M.S., H.E.M., H.H. and L.J.D. performed cell line and biochemical studies. M.G.-C. and C.C. performed tumor xenograft studies. E.L., A.K. and D.L. generated the patient-derived cell lines. H.C.B., V.K.R., C.L.K., D.A.R. and F.S. performed barcode analysis. Y.E.M. and G.G. performed mathematical modeling of *EGFR*^{T790M} evolution. F.J. and R.I.S. performed RNA-seq analysis. A.S.C. performed combination drug screening. G.S., A.J.I. and A.B. performed genotyping analysis. S.R. performed mathematical modeling of emergence of RFP-resistant clones. A.C.F. was involved with study design. L.V.S. and Z.P. provided *EGFR*-mutated NSCLC patient samples. A.N.H. and M.J.N. contributed equally to the study. All authors discussed the results and commented on the manuscript.

COMPETING FINANCIAL INTERESTS

The authors declare competing financial interests: details are available in the online version of the paper.

1. Mok, T.S. *et al.* Gefitinib or carboplatin-paclitaxel in pulmonary adenocarcinoma. *N. Engl. J. Med.* **361**, 947–957 (2009).
2. Maemondo, M. *et al.* Gefitinib or chemotherapy for non-small-cell lung cancer with mutated *EGFR*. *N. Engl. J. Med.* **362**, 2380–2388 (2010).
3. Camidge, D.R., Pao, W. & Sequist, L.V. Acquired resistance to TKIs in solid tumors: learning from lung cancer. *Nat. Rev. Clin. Oncol.* **11**, 473–481 (2014).
4. Sequist, L.V. *et al.* Genotypic and histological evolution of lung cancers acquiring resistance to EGFR inhibitors. *Sci. Transl. Med.* **3**, 75ra26 (2011).

5. Pao, W. *et al.* Acquired resistance of lung adenocarcinomas to gefitinib or erlotinib is associated with a second mutation in the EGFR kinase domain. *PLoS Med.* **2**, e73 (2005).
6. Engelman, J.A. *et al.* MET amplification leads to gefitinib resistance in lung cancer by activating ERBB3 signaling. *Science* **316**, 1039–1043 (2007).
7. Turke, A.B. *et al.* Preexistence and clonal selection of MET amplification in EGFR-mutant NSCLC. *Cancer Cell* **17**, 77–88 (2010).
8. Bhang, H.E. *et al.* Studying clonal dynamics in response to cancer therapy using high-complexity barcoding. *Nat. Med.* **21**, 440–448 (2015).
9. Su, K.Y. *et al.* Pretreatment epidermal growth factor receptor (*EGFR*) T790M mutation predicts shorter EGFR tyrosine kinase inhibitor response duration in patients with non-small-cell lung cancer. *J. Clin. Oncol.* **30**, 433–440 (2012).
10. Ye, X. *et al.* High T790M detection rate in TKI-naive NSCLC with *EGFR*-sensitive mutation: truth or artifact? *J. Thorac. Oncol.* **8**, 1118–1120 (2013).
11. Sharma, S.V. *et al.* A chromatin-mediated reversible drug-tolerant state in cancer cell subpopulations. *Cell* **141**, 69–80 (2010).
12. Lee, H.J. *et al.* Drug resistance via feedback activation of Stat3 in oncogene-addicted cancer cells. *Cancer Cell* **26**, 207–221 (2014).
13. Wilson, T.R. *et al.* Widespread potential for growth factor–driven resistance to anticancer kinase inhibitors. *Nature* **487**, 505–509 (2012).
14. Crystal, A.S. *et al.* Patient-derived models of acquired resistance can identify effective drug combinations for cancer. *Science* **346**, 1480–1486 (2014).
15. Zhou, W. *et al.* Novel mutant-selective EGFR kinase inhibitors against $EGFR^{T790M}$. *Nature* **462**, 1070–1074 (2009).
16. Hata, A.N., Engelman, J.A. & Faber, A.C. The BCL2 family: key mediators of the apoptotic response to targeted anticancer therapeutics. *Cancer Discov.* **5**, 475–487 (2015).
17. Cragg, M.S., Kuroda, J., Puthalakath, H., Huang, D.C. & Strasser, A. Gefitinib-induced killing of NSCLC cell lines expressing mutant EGFR requires BIM and can be enhanced by BH3 mimetics. *PLoS Med.* **4**, 1681–1689, discussion 1690 (2007).
18. Costa, D.B. *et al.* BIM mediates EGFR tyrosine kinase inhibitor–induced apoptosis in lung cancers with oncogenic *EGFR* mutations. *PLoS Med.* **4**, 1669–1679 discussion 1680 (2007).
19. Gong, Y. *et al.* Induction of BIM is essential for apoptosis triggered by EGFR kinase inhibitors in mutant EGFR-dependent lung adenocarcinomas. *PLoS Med.* **4**, e294 2007).
20. Faber, A.C. *et al.* BIM expression in treatment-naive cancers predicts responsiveness to kinase inhibitors. *Cancer Discov.* **1**, 352–365 (2011).
21. Robasky, K., Lewis, N.E. & Church, G.M. The role of replicates for error mitigation in next-generation sequencing. *Nat. Rev. Genet.* **15**, 56–62 (2014).
22. Hindson, B.J. *et al.* High-throughput droplet digital PCR system for absolute quantitation of DNA copy number. *Anal. Chem.* **83**, 8604–8610 (2011).
23. Zheng, Z. *et al.* Anchored multiplex PCR for targeted next-generation sequencing. *Nat. Med.* **20**, 1479–1484 (2014).
24. Ohashi, K. *et al.* Lung cancers with acquired resistance to EGFR inhibitors occasionally harbor *BRAF* gene mutations but lack mutations in *KRAS*, *NRAS* or *MEK1*. *Proc. Natl. Acad. Sci. USA* **109**, E2127–E2133 (2012).
25. Eberlein, C.A. *et al.* Acquired resistance to the mutant-selective EGFR inhibitor AZD9291 is associated with increased dependence on RAS signaling in preclinical models. *Cancer Res.* **75**, 2489–2500 (2015).
26. Piotrowska, Z. *et al.* Heterogeneity underlies the emergence of $EGFR^{T790}$ wild-type clones following treatment of T790M-positive cancers with a third-generation EGFR inhibitor. *Cancer Discov.* **5**, 713–722 (2015).
27. Jänne, P.A. *et al.* AZD9291 in EGFR inhibitor–resistant non-small-cell lung cancer. *N. Engl. J. Med.* **372**, 1689–1699 (2015).
28. Sequist, L.V. *et al.* Rociletinib in EGFR-mutated non-small-cell lung cancer. *N. Engl. J. Med.* **372**, 1700–1709 (2015).
29. Cross, D.A. *et al.* AZD9291, an irreversible EGFR TKI, overcomes T790M-mediated resistance to EGFR inhibitors in lung cancer. *Cancer Discov.* **4**, 1046–1061 (2014).
30. Cragg, M.S. *et al.* Treatment of BRAF–mutant human tumor cells with a MEK inhibitor requires Bim and is enhanced by a BH3 mimetic. *J. Clin. Invest.* **118**, 3651–3659 (2008).
31. Corcoran, R.B. *et al.* Synthetic lethal interaction of combined BCL-XL and MEK inhibition promotes tumor regressions in KRAS-mutant cancer models. *Cancer Cell* **23**, 121–128 (2013).
32. de Bruin, E.C. *et al.* Spatial and temporal diversity in genomic instability processes defines lung cancer evolution. *Science* **346**, 251–256 (2014).
33. McGranahan, N. & Swanton, C. Biological and therapeutic impact of intratumor heterogeneity in cancer evolution. *Cancer Cell* **27**, 15–26 (2015).
34. Misale, S., Di Nicolantonio, F., Sartore-Bianchi, A., Siena, S. & Bardelli, A. Resistance to anti-EGFR therapy in colorectal cancer: from heterogeneity to convergent evolution. *Cancer Discov.* **4**, 1269–1280 (2014).
35. Maheswaran, S. *et al.* Detection of mutations in *EGFR* in circulating lung cancer cells. *N. Engl. J. Med.* **359**, 366–377 (2008).
36. Byers, L.A. *et al.* An epithelial-mesenchymal transition gene signature predicts resistance to EGFR and PI3K inhibitors and identifies Axl as a therapeutic target for overcoming EGFR-inhibitor resistance. *Clin. Cancer Res.* **19**, 279–290 (2013).
37. Hirata, E. *et al.* Intravital imaging reveals how BRAF inhibition generates drug-tolerant microenvironments with high integrin-β1 and FAK signaling. *Cancer Cell* **27**, 574–588 (2015).
38. Ramirez, *et al.* Diverse drug-resistance mechanisms can emerge from drug-tolerant cancer persister cells. *Nat. Commun.* (in the press).
39. Thress, K.S. *et al.* Acquired $EGFR^{C797S}$ mutation mediates resistance to AZD9291 in non-small-cell lung cancer harboring $EGFR^{T790M}$. *Nat. Med.* **21**, 560–562 (2015).

Personnel Effort on Project

Lecia Sequist, Principal Investigator
Anuj Kalsy, Research Specialist
Richard Dicecca, Research Technician
Hilary Mulvey, Research Technician
Melissa Parks, Research Technician
Rosa Frias, Research Technician

ONLINE METHODS

Cell lines. The EGFR-mutant NSCLC PC9 cell line (*EGFR* exon 19, del(E746_A750), *EGFR* amplified) was obtained from the MGH Center for Molecular Therapeutics. The identity of PC9 parental, GR2 and GR3 cell lines were verified by STR analysis (Bio-synthesis, Inc.) at the time that these studies were performed. EGFR-mutant NSCLC patient-derived cell lines were established in our laboratory from core biopsy or pleural effusion samples as previously described[14,40]. The MGH1075 stromal fibroblast line was established in our laboratory from a surgical resection specimen of an early-stage primary lung adenocarcinoma. All patients signed informed consent to participate in a Dana-Farber–Harvard Cancer Center Institutional Review Board–approved protocol giving permission for research to be performed on their samples. The HCC827-GR6 line (exon 19 deletion, MET amplified) was previously described[6]. H358 cells were obtained from the Center for Molecular Therapeutics at MGH. PC9-T790M-RFP and MGH119-GR1-RFP cells were generated by infecting the PC9 Early T-1 clone and MGH119-GR1 cells, respectively, with Cignal Lenti RFP (Qiagen) lentivirus followed by puromycin selection. All cell lines were maintained in RPMI (Life Technologies) supplemented with 10% FBS, except for MGH125 and MGH138 cells, which were maintained in ACL4 medium (Life Technologies) with 10% FBS and TCM (3:1 (vol/vol) F-12 nutrient mixture–Dulbecco's Modified Eagle's Medium (Life Technologies), 5% fetal bovine serum, 0.4 μg/ml hydrocortisone, 5 μg/ml insulin, 8.4 ng/ml cholera toxin, 10 ng/ml epidermal growth factor, and 24 μg/ml adenine), respectively. All experiments were performed in RPMI with 10% FBS. All cells were routinely tested and verified to be free of mycoplasma contamination.

Antibodies and reagents. For western blotting, the following antibodies were used: phospho-EGFR Y1068 (Abcam AB5644), EGFR (Cell Signaling 2646), pERK1/2 T202/204 (Cell Signaling 9101), ERK1/2 (Cell Signaling 9102), p-AKT S473 (Cell Signaling 4060), AKT1/2/3 (Santa Cruz sc-8312), BIM (Cell Signaling 2933), Actin (Cell Signaling 4970). For cell culture studies, gefitinib, WZ4002, NVP-AEW541, and ABT-263 (all from Selleck), were dissolved in DMSO to a final concentration of 10 mmol/liter and stored at −20 °C. Unless otherwise specified, 1 μM concentration was used for *in vitro* cell culture experiments.

***In vitro* generation of gefitinib-resistant cell lines.** Gefitinib-resistant PC9-GR2, PC9-GR3 and MGH119-GR1 cells were established by culturing parental cells in escalating concentrations of gefitinib (10 nM–1 μM), as tolerated, as previously described[14]. MGH119-GR2 cells were established by culturing parental cells in full-dose gefitinib (1 μM). Early, drug-tolerant, late PC9 resistant clones were established by culturing in 300 nM gefitinib until resistant, at which point they were maintained in 1 μM gefitinib. During generation of resistance, medium and drug were replaced twice per week.

Generation of PC9 single-cell subclones. PC9 parental cells were seeded into 96-well plates at a density of 0.5 cells/well. After 2 weeks, approximately 25–40% of wells (50–80% of theoretical yield) contained colonies of about 10,000 cells. A minority of wells contained two colonies, which were easily distinguishable. Wells containing only single colonies were expanded an additional 6–10 doublings for use in experiments.

Propidium iodide and annexin V apoptosis assay. Cells were seeded at low density 24 h before addition of drug. 72 h after adding drugs, floating and adherent cells were collected and stained with propidium iodide and Cy5–annexin V (BD Biosciences) and analyzed by flow cytometry. The annexin V–positive apoptotic cell fraction was analyzed using FloJo software (FlowJo, LLC).

CellTiter-Glo proliferation assay. For dose-response assays, cell lines were seeded into 96-well plates 24 h before addition of drug. Cell proliferation was determined by CellTiter-Glo assay (Promega) 72 h after adding drug, using standard protocols. For time-course experiments, multiple plates were seeded and drugged in identical fashion, and at the indicated time points, the plates were frozen at −80 °C; all plates in an experiment were developed with CellTiter-Glo simultaneously. For early-resistant and drug-tolerant cell experiments, CellTiter-Glo assays were performed at the indicated times on cells *in situ*.

RealTime-Glo viability assay. Cell viability was assayed *in situ* once a week starting the day after seeding, using the RealTime-Glo assay (Promega) according to the manufacturer's protocol. Briefly, MT Cell Viability Substrate and NanoLuc Enzyme were diluted 1:500 in medium, and 25 μl was added to each well (1/5 total final volume). Cells were incubated for 1 h at 37 °C and luminescence was measured. For experiments including RFP-labeled cells, RFP fluorescence was measured using excitation at 553 nm and emission at 574 nm. We did not observe any effect of the presence of RFP on RealTime-Glo luminescence or vice versa. Fresh medium containing gefitinib was used to replace the assay reagents immediately after each assay.

Long-term viability assay. Long-term viability assays were completed by plating 1,000–4,000 cells/well in replicate 96-well plates. Cells were treated in quadruplicate 2× per week and fixed at days 0, 3, 7, 14, 21, 28 and 35 with a mixture of formaldehyde (1.0%), PBST (0.04%), and Hoecsht dye (1 μg/ml). Stained nuclei were imaged and then counted using a Molecular Devices ImageXpress Micro high-content imager and MetaXpress software (Molecular Devices).

Cell cycle analysis. Cells were seeded 24 h before experiment to give a confluency of 30–50%. Drugs were added for 24 h and cells were harvested, stained with propidium iodide and analyzed by flow cytometry. Cell cycle subpopulations were calculated using the cell cycle module in FloJo software.

JC-1 mitochondrial depolarization assay. Cells were treated with EGFR inhibitor in the presence of 10 μM QVD-Oph (Sigma) to prevent subsequent apoptosis. 48 h after drug treatment, cells were harvested and stained with JC-1 dye (Life Technologies) according to the manufacturer's recommendations. Treatment with 10 μM CCCP (2-[2-(3-chlorophenyl)hydrazinylyidene]propanedinitrile; Life Technologies) was used as a positive control. Cells were analyzed by flow cytometry using excitation-emission filters for phycoerythrin (PE) and FITC. Mitochondrial depolarization is indicated by a decrease in the red/green fluorescence intensity ratio.

Quantitative RT-PCR assay for gene expression. Cells were seeded 24 h before give a confluency of 50%. Cells were treated with drugs for 24 h and RNA was extracted using the RNeasy Kit (Qiagen). cDNA was prepared from 500 ng total RNA with the First Strand Synthesis Kit (Invitrogen) using oligo-dT primers. Quantitative PCR was performed using FastStart SYBR Green (Roche) on a Lightcycler 480. mRNA expression relative to actin mRNA levels was calculated using the delta-delta threshold cycle ($\Delta\Delta C_T$) method. Primers used: *DUSP6* F 5′-CGACTGGAACGAGAATACGG-3′, R 5′- TTGGAACTTACTGAAGCCACCT-3′; *SPRY4* F 5′- CCCCGGCTTCAGGATTTA-3′, R 5′-CTGCAAACCGCTCAATACAG-3′; *HER3* F 5′-CTGATCACCGGCCTCAAT-3′, R 5′-GGAAGACATTGAGCTTCTCTGG-3′; *DAPK1* F 5′-CCCTTGTCCCAGTTGAAGAA-3′, R 5′-CCGGTCGAGGAACATTCA-3′; *BIM* F 5′- GATCCTTCCAGTGGGTATTTCTCTT-3′, R 5′-ACTGAGATAGTGGTTGAAGGCCTGG-3′; Actin F 5′-CTGTGCTATCCCTGTACGCCTC-3′, R 5′-CATGATGGAGTTGAAGGTAGTTTCGT-3′; *GAPDH* F 5′-AACAGCGACACCCATCCTC-3′, R 5′-CATACCAGGAAATGAGCTTGACAA-3′.

***EGFR*^{T790M} quantitative-PCR assay.** The *EGFR*^{T790M} mutation was detected using allele-specific primers (F) 5′-ACCATGCGAAGCCACACTGACG-3′ and (R) 5′-AGCCGAAGGGCATGAGCTGGA-3′ in conjunction with an *EGFR* exon 20 Taqman probe 5′-ATCACGTAGGCTTCCTGGAG-3′. A commercially available *EGFR* exon 19–deletion Taqman assay was used as a reference (Hs00000228_mu, Life Technologies). Quantitative PCR was performed on genomic DNA using either FastStart PCR Master or Lightcycler 480 Probes Master kits (Roche) on a Lightcycler 480. For screening assays, ΔCp(T790M-del19) < 8 was considered positive and ΔCp > 10 was considered negative (Probes Master), or ΔCp < 14 was considered positive and ΔCp > 16 was considered negative (FastStart).

***EGFR*^{T790M} droplet digital PCR analysis.** Isolated genomic DNA was amplified using ddPCR Supermix for Probes (Bio-Rad) with EGFR p.T790M (PrimePCR ddPCR Mutation Assay, Bio-Rad) for point-mutation detection. ddPCR was performed according to the manufacturer's protocol, and the results are reported

doi:10.1038/nm.4040

as percentage or fractional abundance of mutant DNA alleles to total (mutant plus wild-type) DNA alleles. 8–10 µl of DNA template was added to 10 µl of ddPCR Supermix for Probes (Bio-Rad) and to 2 µl of the primer-probe mixture. Droplets were generated using Auto-DG where the reaction mix was added together with Droplet Generation Oil for Probes (Bio-Rad). Droplets were then transferred to a 96-well plate (Eppendorf) and then thermal-cycled with the following conditions: 5 min at 95 °C; 40 cycles of 94 °C for 30 s, 55 °C for 1 min; followed by 98 °C for 10 min (ramp rate 2 °C/s). Droplets were analyzed with the QX200 Droplet Reader (Bio-Rad) for fluorescent measurement of FAM (6-carboxyfluorescein) and HEX (hexachlorofluorescein) dye probes. Gating was performed based on positive and negative controls, and mutant populations were identified. The ddPCR data were analyzed with QuantaSoft analysis software (Bio-Rad) to obtain fractional abundance of the mutant DNA alleles in the wild-type or normal background. Fractional abundance is calculated as follows: F.A. % = $((N_{Mut} / (N_{Mut} + N_{WT})) \times 100)$, where N_{Mut} is number of mutant events and N_{WT} is number of wild-type (WT) events per reaction. ddPCR analysis of normal control (from cell lines) and no–DNA template controls were always included. Samples with a low number of positive events were repeated at least twice in independent experiments to validate the obtained results.

Clinical genotyping assay. DNA was extracted from late, gefitinib-resistant *EGFR*^{T790M}-negative PC9 clones using the DNeasy kit (Qiagen). Genotyping was performed using the MGH NGS platform, which utilizes a multiplex polymerase chain reaction (PCR) technology called Anchored Multiplex PCR (AMP) for single-nucleotide variant (SNV) and insertion-deletion (indel) detection in genomic DNA using next-generation sequencing (NGS). Genomic DNA was sheared with the Covaris M220 instrument, followed by end-repair, adenylation, and ligation with an adaptor. A sequencing library targeting hotspots and exons in 39 genes was generated using two hemi-nested PCR reactions. Illumina MiSeq 2 × 151 base paired-end sequencing results were aligned to the hg19 human genome reference using BWA-MEM. MuTect and a laboratory-developed insertion-deletion analysis algorithm were used for SNV and indel variant detection, respectively. This assay has been validated to detect SNV and indel variants at 5% allelic frequency or higher in target regions with sufficient read coverage. Variants are reported with Human Genome Variation Society (HGVS) protein and DNA nomenclature, followed by the referenced Ensembl transcript ID. The gene targets covered by this assay are as follows (exons in parentheses): *AKT1* (3), *ALK* (22, 23, 25), *APC* (16), *BRAF* (11, 15), *CDH1* (1, 2, 3, 4, 5, 6, 7, 8, 9, 10, 11,12, 13, 14, 15, 16), *CDKN2A* (1, 2, 3), *CTNNB1* (3), *DDR2* (12, 13, 14, 15, 16, 17, 18), *EGFR* (7, 15, 18, 19, 20, 21), *ERBB2* (10, 20), *ESR1* (8), *FBXW7* (1, 2, 3, 4, 5, 6, 7, 8, 9, 10, 11), *FGFR1* (4, 8, 15, 17), *FGFR2* (7, 9, 12,14), *FGFR3* (7, 8, 9, 14, 16), *FOXL2* (1), *GNA11* (5), *GNAQ* (4, 5), *GNAS* (6, 7, 8, 9), *HRAS* (2, 3), *IDH1* (3, 4), *IDH2* (4), *KIT* (8, 9, 11, 17), *KRAS* (2, 3, 4, 5), *MAP2K1* (2, 3), *MET* (14, 16, 19, 21), *NOTCH* (25, 26, 34), *NRAS* (2, 3, 4, 5), *PDGFRA* (12, 14, 18, 23), *PIK3CA* (2, 5, 8, 10, 21), *PIK3R1* (1, 2, 3, 4, 5, 6, 7, 8, 9, 10), *PTEN* (1, 2, 3, 4, 5, 6, 7, 8, 9), *RET* (11, 16), *ROS1* (38), *SMAD4* (2, 3, 4, 5, 6, 7, 8, 9, 10, 11, 12), *SMO* (9), *STK11* (1, 2, 3, 4, 5, 6, 7, 8, 9), *TP53* (1, 2, 3, 4, 5, 6, 7, 8, 9, 10, 11), and *VHL* (1, 2, 3).

Gene amplification quantitative PCR assay. Quantitative PCR was performed on genomic DNA using FastStart Sybr Green (Roche) on a Lightcycler 480. Primers for *KRAS*, *MET*, a chromosome 12 control and a chromosome 7 control were previously described[41]. *EGFR*, *BRAF* and *NRAS* primers were adapted from Dias-Santagata *et al.*[42]: *EGFR* F 5′-CCTCCTTCTGCATGGTATTC-3′, R 5′- GCAGCATGTCAAGATCACAG-3′; *BRAF* F 5′- TGCTTGCTCTGATAGGAAAATG-3′, R 5′- CTGATGGGAC CCACTCCAT-3′; *NRAS* F 5′- CAACAGGTTCTTGCTGGTGT-3′, R 5′-GAGAGACAGGATCAGGTCAGC-3′. *LINE1* primers: F 5′-AAAGCCGCT CAACTACATGG -3′, R 5′-TGCTTTGAATGCGTCCCAGAG -3′. ΔCp between gene-control pairs (*KRAS*–chr. 12, *LINE1*; *MET*, *EGFR*, *BRAF*–chr. 7, *LINE1*; *HER2*, *NRAS*–*LINE1*) were calculated and normalized to ΔCp from a MGH1075 diploid fibroblast control. HCC827-GR6 cells were used as a *MET*-amplification control[6] and H358 cells were used as *KRAS*-amplification control.

Generation of tetracycline-inducible *EGFR* pTREX cell lines. Plasmids encoding *EGFR* with and exon 19 deletion (del) and *EGFR*^{T790M} with an exon 19 del were purchased from Addgene (32062 and 32072, respectively). *EGFR* sequences were PCR-amplified with the F 5′-CACCATGCGACCCTCCGGGACG-3′ and R 5′-TCATGCTCCAATAAATTCACTG-3′ primers and ligated into the pENTR/D-TOPO vector using the pENTR Directional TOPO Cloning Kits (Invitrogen). The sequence was then introduced into the pTREX vector (kindly provided by Novartis) using Gateway LR Clonase Enzyme (Invitrogen). The pTREX-DEL19 and pTREX-DEL/T790M vectors were subsequently verified by DNA sequencing. Lentivirus was produced using standard procedures[43]. PC9 and MGH119 cells were infected with lentivirus followed by puromycin selection. Cells were cultured in the presence of 10 ng/ml doxycycline to induce expression of the *EGFR* construct. For infection of PC9 drug-tolerant single cells, cells were infected with a lentiviral titer that yielded a single puromycin-resistant colony in ~50% of wells.

Mouse xenograft studies. All mouse studies were conducted through Institutional Animal Care and Use Committee–approved animal protocols in accordance with institutional guidelines (MGH Subcommittee on Research Animal Care, OLAW Assurance A3596-01). For xenograft studies, cell line suspensions were prepared in 1:10 matrigel and 5×10^6 cells were injected subcutaneously into the flanks of female athymic nude (Nu/Nu) mice (6–8 weeks old). Visible tumors developed in approximately 2–4 weeks. Tumors were measured with electronic calipers and the tumor volume was calculated according to the formula $Vol = 0.52 \times L \times W^2$. Mice with established tumors were randomized to drug-treatment groups using covariate-adaptive randomization to minimize differences in baseline tumor volumes: WZ4002 at 50 mg/kg (10% 1-methyl-2-pyrolidone, 90% PEG300), ABT-263 at 100 mg/kg (30% PEG400, 60% Phosal 50 PG, 10% ethanol), or combinations thereof. Drug treatments were administered by oral gavage and tumor volumes were measured twice weekly, as described above. For pharmacodynamic studies, mice were sacrificed, and tumors were removed 3 h after drug administration on day 3. Tumors were snap-frozen, and lysates were prepared for western blotting. Investigators performing tumor measurements were not blinded to treatment groups. Sample size (minimum $n = 7$ per treatment group) was chosen to verify satisfactory interanimal reproducibility.

Estimation of frequency of pre-existing *EGFR*^{T790M} clones in parental PC9 cells. After 2 weeks of drug exposure, 90 of 1,260 wells were detected to contain resistant *EGFR*^{T790M} colonies. Based on the above modeling of emergence of pre-existing RFP-labeled *EGFR*^{T790M} clones, this represents approximately 72% of pre-existing *EGFR*^{T790M} cells. Thus the theoretical frequency of pre-existing *EGFR*^{T790M} can be estimated:

$$\frac{(90 \text{ colonies} / 0.7259)}{1{,}260 \text{ wells} \times 5{,}000 \text{ cells/well}} = 0.00001968 \approx 1{:}50{,}000$$

From experiments generating PC9 single-cell clones, the efficiency of single PC9 cells to establish progeny is between 50% and 80%, thus the frequency of *EGFR*^{T790M} cells in our parental PC9 line is approximately 1:25,000–1:50,000.

ClonTracer barcode library. Construction of the ClonTracer barcode library and generation of lentiviral particles was previously described[8]. Pools of 10 million PC9 cells were barcoded by lentiviral infection at a multiplicity of infection (MOI) of 0.1–0.2, and infected cells were selected with puromycin. Infected cell populations were expanded in culture for the minimal time period to obtain a sufficient number of cells to set up replicate experiments. 20 million cells (~10× barcode representation) were seeded in multiple replicate plates and treated with vehicle or 300 nM gefitinib (five replicates). Vehicle-treated cells reached confluency within 3 d and the entire pool was pelleted and snap-frozen. Gefitinib-treated plates became confluent from the emergence of early-resistant clones and were harvested after 3 weeks. Cell counts were approximately 20 million cells per replicate plate. Genomic DNA was extracted from the frozen cell populations with a QIAamp DNA Blood Maxi Kit (Qiagen). We used PCR to amplify the barcode sequence for NGS and introduce Illumina adaptors and index sequences[8]. PCR primer sequence information can be found at https://www.addgene.org/pooled-library/clontracer/. The sampling of sufficient template coverage was ensured by parallel PCR reactions.

PCR-amplified products were sequenced on an Illumina HiSeq2500 sequencer in rapid mode using the 50 Cycle TruSeq Rapid v2 SBS Kit, TruSeq Rapid SR v2 Cluster Kit, and HiSeq Rapid SR v2 Flow Cell (Illumina) as previously described[8]. Barcode-composition analysis was carried out as previously described[8]. A barcode was called significant if it was seen at more than 0.01% of the total population in the drug-treated samples (10 times the fraction of the most enriched barcode in the vehicle-treated replicates).

Cumulative density function modeling of emergence of *EGFR*^{T790M} clones. Using the cumulative number (N) of RFP$^+$ clones detected at each time point, a best-fit model (without being highly sensitive to local noise) was calculated with the Matlab Curve Fitting Tool with fittype exp2, representing a model of the form $a \times \exp^{(b \times x)} + c \times \exp^{(d \times x)}$. The 95% confidence bounds for the coefficients of equation (1) were: $a = 53.56$ (47.19, 59.93), $b = 0.0002647$ (−0.001714, 0.002243), $c = -53.58$ (−60.17, −47), and $d = -0.09483$ (−0.1178, −0.07186), where the variable x represents time (t). The equation:

$$ft = 53.56e^{0.0002647t} - 53.58e^{-0.09483t}$$
$$r^2 = 0.9981$$

was normalized by the value $f(70) = 54.492$, transforming it into a cumulative density function with values ranging from [0,1]:

$$\frac{53.56e^{0.0002647t} - 53.58e^{-0.09483t}}{54.492}$$

The value of the CDF at t(14 d) = 0.7259, representing the probability that a pre-existing *EGFR*^{T790M} clone would emerge within 14 d. The probability that a pre-existing *EGFR*^{T790M} clone would not emerge within 14 d is 1 − 0.7259 = 0.2741. The probability of this occurring in four independent trials = $(0.2741)^4 = 0.0056$.

Mathematical modeling of *EGFR*^{T790M} evolution from drug-tolerant cells. To model *de novo* acquisition of the *EGFR*^{T790M} mutation during drug treatment, we assumed a branching process[44] comprised of N_0 drug tolerant cells that divide at a rate b, die at rate d, and upon birth, mutate at a rate μ. Acquisition of *EGFR*^{T790M} mutations yields resistant cells that divide at a rate of b_r and die at a rate d_r. The range of values of the birth and death rates of drug-tolerant cells were based on single-cell parameters reported by Tyson *et al.*[45] and fit to population growth rates determined by tracking the growth of pools of PC9 drug-tolerant cells during weeks 5–11 of gefitinib treatment (**Supplementary Fig. 9a**). The average estimated growth rate determined by fitting the growth curves to an exponential function from the week with the smallest population, which was usually week 6 until week 11, and taking the average was $b - d = 0.0015 \pm (0.0012)$/h. Using the inferred growth rate we back-extrapolated the initial population size of the drug-tolerant cells to be on average $N_0 = 150 \pm 23$. Once a cell acquired the *EGFR*^{T790M} mutation, the birth and death rate of the resulting *EGFR*^{T790M} cells were assumed to be similar to those of the PC9 parental cells in the absence of drug (Tyson *et al.*[45]). Currently there is no agreement on the average mutation per SNV per cell division, and estimation ranges from 10^{-11} up to 10^{-7} for non-hypermutated cells[46,47]. More recent estimates range from 10^{-10} to 10^{-8} (ref. 48), with a slight tendency toward lower values. Of note, the *EGFR*^{T790M} mutation is a change from ACG to ATG—generated by spontaneous deamination of 5-methylcytosine to uracil, which occurs at 18 times greater than the average rate[48]; furthermore the *EGFR* gene has a mutation rate that is about twice the average rate[49] across the genome (MutSigCV[50] estimation output). Gene amplification can increase the allelic pool in which a mutation can arise, and PC9 cells have an amplification of the *EGFR* gene (10 copies per cell; see **Supplementary Fig. 4b**) with a single *EGFR*^{T790M} mutation being sufficient to confer drug resistance. Effectively, the rate of getting an *EGFR*^{T790M} mutation is about 360 times higher than that of an average SNV.

We modeled the process with a Monte Carlo simulation in order to estimate the fraction of drug-tolerant pools predicted to acquire *EGFR*^{T790M} by 16 weeks after beginning drug treatment. Conversely, we simulated the fraction of drug-tolerant pools predicted to acquire *EGFR*^{T790M} as a function of time, using fixed parameters. Additionally we derived an analytical approximation to the model

$$R = 1 - (1-\mu)\frac{N_0 e^{(b-d)T}}{b-d}b \sim \frac{N_0 e^{(b-d)T}}{b-d}b\mu$$

where R represents the fraction of PC9 drug-tolerant pools that acquire an *EGFR*^{T790M} mutation as a function of time (T). Parameters for drug-tolerant cells: initial population size $N_0 = 150$, birth rate $b = 0.0162$, death rate $d = 0.015$, mutation rate $\mu = 7 \times 10^{-10}$ (estimated to be the average of many estimates by Lynch[49]). The birth and death rates of *EGFR*^{T790M}-mutated cells are $b_r = 0.04$ and $d_r = 0.0015$, respectively[45]. In **Supplementary Figure 9**, we compare the results of the analytical solution (black line) to the Monte Carlo simulations (red dots) based on 10,000 runs per set of values. The logic behind the solution is to estimate the number of birth events from day 0 to the end of the experiment, which is

$$\frac{N_0 e^{(b-d)T}}{b-d}b$$

and calculate the probability of having at least one *EGFR*^{T790M} mutation. One should have in mind that the mutation rate in the equation is not the average mutation per SNV per cell division, but rather, it is 360 times higher, as explained above. It is possible that prior models may not have taken this into account, which may explain the differences in the assumed baseline mutational rates between our model and prior models (for example, 10^{-8}–10^{-7}) (ref. 44).

RNA-seq analysis. Total RNA was isolated using the RNeasy Mini Kit (Qiagen). RNA-seq libraries were constructed from polyadenosine (polyA)-selected RNA using NEBNext Ultra Directional RNA library prep kit for Illumina (New England BioLabs) and sequenced on an Illumina HiSeq2500 instrument, resulting in approximately 34 million reads per sample on average. The data have been deposited in NCBI's Gene Expression Omnibus and are accessible through GEO Series accession number GSE75602. STAR aligner[51] was used to map sequencing reads to transcripts in the human hg19 reference genome. Read counts for individual transcripts were produced with HTSeq-count[52], followed by the estimation of expression values and detection of differentially expressed transcripts using EdgeR[53]. Principle component analysis (PCA) was performed on the union of differentially expressed transcripts in all samples. We used the package for gene-set enrichment analysis (GSEA)[54,55] to analyze the enrichment of functional gene groups among differentially expressed transcripts. Normalized enrichment score (NES) and enrichment plots were calculated based on gene lists ranked by the expression ratio between early (parental PC9 and PC9-GR2) and late (PC9-GR3 and drug tolerant) stages.

Combination drug screen. The combination drug-screening platform has been described previously[14]. Briefly, the panel of screened compounds was comprised of 76 targeted agents directed against a broad range of biologic targets including regulators of growth factor and development signaling pathways, apoptosis, transcription and protein folding, and DNA damage. Cells were treated with vehicle or varying concentrations of drugs to be screened (10,000-fold range), in the absence or presence of 1 μM WZ4002, for 72 h, and cell viability was determined by the CellTiter-Glo assay. Each dose-response curve was normalized to the cell viability of corresponding vehicle-treated cells (with or without WZ4002 treatment). For each dose of a drug in the screen, a ΔE was calculated:

$$\Delta E = 1 - (\text{viability}_{(+WZ)} / \text{viability}_{(-WZ)})$$

The means of the three highest ΔE values for all of the screened drugs were ranked, and screened drugs that scored 0.20 or higher in at least two of four cell lines were identified.

Data and statistical analysis. Data were analyzed using GraphPad Prism software (GraphPad Software). Unless otherwise specified, data displayed are mean ± s.e.m. Pairwise comparisons between groups (for example, experimental versus control) were made using paired or unpaired Student's t-tests as appropriate.

doi:10.1038/nm.4040

For xenograft tumor measurements, individual time points were compared using multiple *t*-tests with Sidak-Bonferroni correction for multiple comparisons. For xenograft pharmacodynamic studies, unequal variance between groups was observed in a minority of cases, so a Welch correction was performed for all comparisons. For all other experiments, the variance between comparison groups was verified to be equivalent. Unless otherwise indicated, $P < 0.05$ was considered to be statistically significant.

40. Niederst, M.J. *et al.* RB loss in resistant EGFR-mutant lung adenocarcinomas that transform to small-cell lung cancer. *Nat. Commun.* **6**, 6377 (2015).
41. Misale, S. *et al.* Blockade of EGFR and MEK intercepts heterogeneous mechanisms of acquired resistance to anti-EGFR therapies in colorectal cancer. *Sci. Transl. Med.* **6**, 224ra26 (2014).
42. Dias-Santagata, D. *et al.* Rapid targeted mutational analysis of human tumors: a clinical platform to guide personalized cancer medicine. *EMBO Mol. Med.* **2**, 146–158 (2010).
43. Hata, A.N. *et al.* Failure to induce apoptosis via BCL-2 family proteins underlies lack of efficacy of combined MEK and PI3K inhibitors for KRAS-mutant lung cancers. *Cancer Res.* **74**, 3146–3156 (2014).
44. Chmielecki, J. *et al.* Optimization of dosing for EGFR-mutant non-small-cell lung cancer with evolutionary cancer modeling. *Sci. Transl. Med.* **3**, 90ra59 (2011).
45. Tyson, D.R., Garbett, S.P., Frick, P.L. & Quaranta, V. Fractional proliferation: a method to deconvolve cell population dynamics from single-cell data. *Nat. Methods* **9**, 923–928 (2012).
46. Kunkel, T.A. & Bebenek, K. DNA replication fidelity. *Annu. Rev. Biochem.* **69**, 497–529 (2000).
47. Oller, A.R., Rastogi, P., Morgenthaler, S. & Thilly, W.G. A statistical model to estimate variance in long-term, low-dose mutation assays: testing of the model in a human lymphoblastoid mutation assay. *Mutat. Res.* **216**, 149–161 (1989).
48. Alexandrov, L.B. *et al.* Signatures of mutational processes in human cancer. *Nature* **500**, 415–421 (2013).
49. Lynch, M. Rate, molecular spectrum and consequences of human mutation. *Proc. Natl. Acad. Sci. USA* **107**, 961–968 (2010).
50. Lawrence, M.S. *et al.* Mutational heterogeneity in cancer and the search for new cancer-associated genes. *Nature* **499**, 214–218 (2013).
51. Dobin, A. *et al.* STAR: ultrafast universal RNA-seq aligner. *Bioinformatics* **29**, 15–21 (2013).
52. Anders, S., Pyl, P.T. & Huber, W. HTSeq—a Python framework to work with high-throughput sequencing data. *Bioinformatics* **31**, 166–169 (2015).
53. Robinson, M.D., McCarthy, D.J. & Smyth, G.K. edgeR: a Bioconductor package for differential expression analysis of digital gene-expression data. *Bioinformatics* **26**, 139–140 (2010).
54. Subramanian, A. *et al.* Gene-set enrichment analysis: a knowledge-based approach for interpreting genome-wide expression profiles. *Proc. Natl. Acad. Sci. USA* **102**, 15545–15550 (2005).
55. Mootha, V.K. *et al.* PGC-1α–responsive genes involved in oxidative phosphorylation are coordinately downregulated in human diabetes. *Nat. Genet.* **34**, 267–273 (2003).